

FEDADAVR: Adaptive Variance Reduction for Robust Federated Learning under Limited Client Participation

S M Ruhul Kabir Howlader¹ Xiao Chen¹ Yifei Xie² Lu Liu³

Abstract

Federated learning (FL) encounters substantial challenges due to heterogeneity, leading to gradient noise, client drift, and partial client participation errors, the last of which is the most pervasive but remains insufficiently addressed in current literature. In this paper, we propose FEDADAVR, a novel FL algorithm aimed at solving heterogeneity issues caused by sporadic client participation by incorporating an adaptive optimiser with a variance reduction technique. This method takes advantage of the most recent stored updates from clients, even when they are absent from the current training round, thereby emulating their presence. Furthermore, we propose FEDADAVR-QUANT, which stores client updates in quantised form, significantly reducing the memory requirements (by 50%, 75%, and 87.5%) of FEDADAVR while maintaining equivalent model performance. We analyse the convergence behaviour of FEDADAVR under general nonconvex conditions and prove that our proposed algorithm can eliminate partial client participation error. Extensive experiments conducted on multiple datasets, under both independent and identically distributed (IID) and non-IID settings, demonstrate that FEDADAVR consistently outperforms state-of-the-art baseline methods.

1. Introduction

The successful deployment of machine learning models hinges upon access to large-scale, high-quality datasets; however, assembling such datasets poses considerable challenges. In healthcare contexts, for instance, the centralised collection of patient data and the training of machine learn-

ing models are constrained by regulations such as the Health Insurance Portability and Accountability Act (HIPAA) and the General Data Protection Regulation (GDPR) (Warnat-Herresthal et al., 2021). Federated Learning (FL) has emerged as an effective paradigm to address these constraints, enabling multiple clients to collaboratively train a shared model without exposing raw data beyond the owner’s device.

The cross-device FL setting (Kairouz et al., 2019) encompasses vast numbers of clients, only a subset of which are active in any given round, resulting in increased heterogeneity in both data distributions and device capabilities, thereby complicating FL training. Moreover, such heterogeneous (non-IID) data give rise to client-drift errors. Convergence analyses of FedAvg (McMahan et al., 2017) have shown that data heterogeneity can slow convergence and introduce bias into the global model (i.e., client drift from non-IID data) (Karimireddy et al., 2020; Li et al., 2020c; Khaled et al., 2020). To counteract these effects, FedProx incorporates a proximal term into the local objective to penalise deviation from the global model (Li et al., 2020b), whereas SCAFFOLD employs control variates to correct client drift error induced by heterogeneity (Karimireddy et al., 2020). Subsequent methods, including ADACOMM (Wang & Joshi, 2019), FedBug (Kao & Wang, 2023), AdaBest (Varno et al., 2022) and Def-KT (Li et al., 2022a), have further refined techniques for mitigating drift. Additionally, several studies have examined client unavailability arising from device and communication variability (Gu et al., 2021; Jhunjhunwala et al., 2022; Su et al., 2023; Wang et al., 2023; Mansour et al., 2023). In summary, FL is primarily affected by client drift and partial participation. The issue of client drift has been extensively studied and was addressed earlier. Consequently, our primary contribution focuses on mitigating the latter challenge, which is introduced in the following paragraph.

The partial client participation error arises from client unavailability. Several studies have investigated this issue in the context of device and communication variability (Gu et al., 2021; Jhunjhunwala et al., 2022; Su et al., 2023; Wang et al., 2023; Mansour et al., 2023). To mitigate this challenge, MIFA was proposed (Gu et al., 2021), which ap-

¹School of Computing and Mathematical Sciences, University of Leicester, UK ²School of Informatics, University of Edinburgh, UK ³Department of Computer Science, University of Exeter, UK. Correspondence to: S M Ruhul Kabir Howlader <smrk1@leicester.ac.uk>, Xiao Chen <xiao.chen@leicester.ac.uk>.

proximates full participation by retaining each client’s most recent update on the server and reusing it in subsequent rounds when that client is unavailable. FedVARP advances this approach by addressing two key limitations of MIFA and demonstrating improved empirical performance. Moreover, it provides a decomposition of the total heterogeneity error into three components: stochastic gradient error, client drift error, and partial participation error. The partial participation error, although significant, has received comparatively limited attention (Jhunjhunwala et al., 2022). Most noteworthy, partial client participation skews the global model update towards the data distributions of the selected subset of clients in each round, thereby exacerbating overall heterogeneity. To reduce the substantial storage overhead associated with maintaining per-client updates at scale, the ClusterFedVARP variant, introduced in (Jhunjhunwala et al., 2022), groups client updates into clusters. This clustering strategy mitigates memory demands without sacrificing convergence performance. However, it may also introduce potential challenges, including incorrect cluster assignments (misgrouped updates), imbalanced cluster sizes, and temporal changes in cluster membership (cluster drift).

Despite the advantages of FedVARP, our previous experiments reveal that it converges slowly under severely label-quantity skew conditions (e.g., when each client’s dataset contains only one or two features). This limitation arises primarily from the fixed server learning rate, resulting in a total absence of adaptivity. In federated settings with partial client participation, certain parameters undergo significantly more frequent updates than others, leading to imbalance. Adaptive optimisers address this issue by modulating individual learning rates based on historical gradient information, thereby enabling larger updates for infrequently adjusted yet crucial parameters while tempering updates for excessively volatile ones (Duchi et al., 2011). Furthermore, under non-IID client distributions, adaptive methods normalise the influence of heterogeneous data, thereby reducing bias towards dominant patterns (Reddi et al., 2021). These insights, alongside the demonstrated effectiveness of SAGA-style variance reduction (VR) techniques (Defazio et al., 2014) and the adaptive optimisation strategies, motivate our proposal to integrate adaptive optimiser on server-side with VR. This paper makes the following contributions:

- We propose FEDADAVR (**F**EDerated **A**DAptivity to **V**ariance **R**eduction), a novel federated learning algorithm that integrates a server-side adaptive optimiser with a SAGA-like VR technique. This design addresses the variance induced by limited client participation, thereby mitigating the impact of client unavailability. The algorithm utilises stored updates of inactive clients, thereby enhancing the robustness of the aggregation process.

- We further introduce FEDADAVR-QUANT, a complementary variant wherein the most recent client updates are retained in quantised form to reduce server-side memory usage (by 50% (FP16), 75% (Int8), and 87.5% (Int4)). Experimental evidence indicates that this quantisation leads to identical performance while substantially reducing memory overhead.
- Comprehensive experiments are carried out under various IID and non-IID data partitioning schemes on multiple datasets, simulating scenarios of extreme client unavailability. The results consistently demonstrate that both FEDADAVR and FEDADAVR-QUANT outperform existing state-of-the-art methods across nearly all experimental configurations.

While prior research has leveraged quantisation primarily to address communication heterogeneity (Reisizadeh et al., 2020; Mao et al., 2022; Ren et al., 2023; Chen et al., 2024) and device constraints (Gupta et al., 2023; Abdelmoniem & Canini, 2021; Chen et al., 2024), to the best of our knowledge, FEDADAVR-QUANT is the first FL strategy to explicitly mitigate server-side memory bottlenecks via the quantisation of stored client states. Uniquely, our approach tackles the challenge of partial client participation by unifying server-side adaptive optimisation, SAGA-style variance reduction, and quantised state maintenance, all backed by formal convergence guarantees.

2. Related Work

Federated Learning. FedAvg (McMahan et al., 2017) is the foundational algorithm in federated learning, wherein a server initialises a global model and dispatches it to clients, who perform several steps of local training using their private data. Clients subsequently return their local updates, which the server aggregates to form an updated global model. This process iterates until convergence. Following FedAvg, numerous FL algorithms have been introduced to address its inherent limitations and the broader challenges within FL. For an overview of these challenges, we refer the reader to (Li et al., 2020a; Rahman et al., 2021; Wen et al., 2022; Guendouzi et al., 2023).

Adaptive Optimisers. Prior to the advent of federated learning, adaptive optimisers such as Adam (Kingma & Ba, 2014) and Adagrad (Duchi et al., 2011) were widely recognised for their effectiveness in guiding convergence behaviour. Building upon this success, the authors of FedOpt (Reddi et al., 2021) pioneered the integration of adaptive optimisers (e.g., Adagrad (Duchi et al., 2011), Adam (Kingma & Ba, 2014), and Yogi (Zaheer et al., 2018)) into federated settings. In the FedOpt family of algorithms, stochastic gradient descent (SGD) is retained on the client side to

preserve communication parity with FedAvg, while three distinct adaptive methods (i.e. FedAdagrad, FedAdam, and FedYogi) are employed on the server side (Reddi et al., 2021). The Lamb optimiser (You et al., 2020) was subsequently utilised to develop FedLamb (Karimi et al., 2023), whereas the AmsGrad optimiser (Reddi et al., 2018) was adopted in a separate FL algorithm (Chen et al., 2020).

Variance Reduction Techniques. Variance reduction techniques have emerged as potent tools for accelerating the convergence of stochastic optimisation by mitigating gradient noise. In SAGA (Defazio et al., 2014), for instance, a table of past gradients is maintained and updated to construct an unbiased estimator at each iteration, yielding linear convergence for strongly convex functions without requiring full-batch gradients. Related methods include SAG (Schmidt et al., 2013), which averages stored gradients to reduce variance. SVRG (Johnson & Zhang, 2013) avoids storage overhead by alternating between full-gradient snapshots and inner stochastic loops. SARAH (Nguyen et al., 2017) further refines this approach by employing recursive gradient estimators without necessitating full-batch gradients. Numerous other VR methods have been proposed for centralised stochastic problems without requiring additional memory. In the context of FL, these methods are generally classified into two categories: *SVRG-style Variance Reduction*, which necessitates client participation in specific rounds, and *Momentum-based Variance Reduction*, which incurs both double communication and double computation costs (Jhunjhunwala et al., 2022). AdaLVR combines variance reduction with Adagrad optimiser to enhance finite-sum optimisation performance (Batardière & Kwon, 2023). Our proposed algorithms are influenced by AdaLVR but are designed to avoid the aforementioned drawbacks.

Quantisation. Quantisation refers to the process of reducing the numerical precision of model parameters to produce a more compact version of the same neural network. Various quantisation techniques have previously been employed to address diverse FL challenges, particularly communication heterogeneity (Reisizadeh et al., 2020; Mao et al., 2022; Ren et al., 2023; Chen et al., 2024), and device heterogeneity (Gupta et al., 2023; Abdelmoniem & Canini, 2021; Chen et al., 2024). The FEDADAVR-QUANT variant of our algorithm employs quantisation to store the most recent client updates, enabling their reuse in subsequent training rounds. To demonstrate the practical feasibility of our approach, we evaluated three fundamental and computationally efficient formats: FP16, Int8, and Int4. While diverse integer quantisation methods exist in the literature, FEDADAVR-QUANT specifically adopts the 8-bit symmetric per-tensor uniform quantiser proposed by (Krishnamoorthi, 2018) and the 4-bit methodology of (Zhou et al., 2016), which packs two 4-bit values per byte for storage.

3. Preliminaries

Federated learning involves a network of N distributed clients (e.g., mobile devices or edge sensors), each possessing a private dataset $\mathcal{D}_n = \{(x_i, y_i)\}$, with no exchange of raw data. The overarching objective is to learn a shared model $w \in \mathbb{R}^d$ by minimising the aggregate empirical loss:

$$\begin{aligned} \min_w F(w) &= \sum_{n=1}^N p_n F_n(w), \\ F_n(w) &= \frac{1}{|\mathcal{D}_n|} \sum_{(x_i, y_i) \in \mathcal{D}_n} \ell(w; x_i, y_i), \end{aligned} \quad (1)$$

where $p_n = \frac{|\mathcal{D}_n|}{\sum_{j=1}^N |\mathcal{D}_j|}$ represents the weight assigned to each client's contribution, and $\ell(\cdot)$ denotes the loss function. Owing to communication and privacy constraints, clients perform several local updates (typically stochastic gradient steps) on $F_n(w)$, and transmit only model updates (rather than raw data) to a central server. The server then aggregates these updates (e.g., through weighted averaging) to produce an improved global model. This federated framework aims to balance statistical heterogeneity (i.e., non-IID data across clients), limited communication bandwidth, and stringent data privacy requirements. Consider the FedAvg algorithm,

Algorithm 1 DEVICEUPDATE($i, \mathbf{w}^{(t)}, \eta_c$)

```

1:  $\mathbf{w}_i^{(t,0)} \leftarrow \mathbf{w}^{(t)}$ 
2: for local step  $k = 0, 1, \dots, K - 1$  do
3:   Compute stochastic gradient  $\nabla f_i(\mathbf{w}_i^{(t,k)})$ 
4:    $\mathbf{w}_i^{(t,k+1)} \leftarrow \mathbf{w}_i^{(t,k)} - \eta_c \nabla f_i(\mathbf{w}_i^{(t,k)})$ 
5: end for
6: return  $\frac{1}{\eta_c} (\mathbf{w}^{(t)} - \mathbf{w}_i^{(t,K)})$ 

```

in which the server randomly selects a subset $\mathcal{S}^{(t)}$ of clients and transmits the current global model $\mathbf{w}^{(t)}$ to them. Each selected client (client id i) then performs the DEVICEUPDATE procedure (see Algorithm 1). The resulting updates, computed as

$$\mathbf{g}_i^{(t)} = \frac{1}{\eta_c} (\mathbf{w}^{(t)} - \mathbf{w}_i^{(t,K)}), \quad (2)$$

where η_c denotes the client learning rate, are subsequently returned to the server. The server aggregates these local updates to form the new global model according to:

$$\mathbf{w}^{(t+1)} = \mathbf{w}^{(t)} - \sum_{i \in \mathcal{S}^{(t)}} p_i \mathbf{g}_i^{(t)}. \quad (3)$$

Variance arises in this process due to the random selection of clients, particularly when their local datasets are heterogeneous. Classical federated learning algorithms like

FedAvg (McMahan et al., 2017) struggle to manage this variance in scenarios where only a small number of clients participate per round and the data distribution is highly skewed.

4. FEDADAVR and FEDADAVR-QUANT

This section introduces the proposed algorithms, FEDADAVR and FEDADAVR-QUANT, both designed to address variance resulting from limited client participation and highly skewed data distributions across clients. The proposed method combines the variance reduction capability of SAGA with the adaptive characteristics of optimisers such as Adam, Adagrad, Adabelief, Yogi, and Lamb. Within FEDADAVR, the server employs an adaptive optimiser in conjunction with a variance reduction strategy. Notably, the proposed FEDADAVR, as defined in Algorithm 2, operates using only the gradients exchanged between the server and the clients, imposing no additional computational or communication burden on client devices.

During each training round, a subset $S^{(t)}$ of clients is randomly selected under the FEDADAVR framework. The selected clients receive the global model $\mathbf{w}^{(t)}$ from the server and carry out local stochastic gradient descent (SGD). Following this, each participating client transmits its local update $\mathbf{g}_i^{(t)}$ to the server. Up to this stage, the procedure mirrors that of FedAvg. However, whereas FedAvg applies direct averaging of client updates (see eq. (3)), it is susceptible to high variance under limited client participation when data distributions are heterogeneous. This source of variance constitutes the dominant error component. To mitigate this, the proposed method incorporates a variance reduction mechanism in conjunction with an adaptive optimiser. The server retains the most recent update received from each client, thereby simulating full client presence in each round. In the quantised variant, referred to as FEDADAVR-QUANT, the stored updates are quantised to reduce memory usage, while all other components remain consistent with those of FEDADAVR.

The server maintains the most recent updates received from clients. Initially, each client $j \in [N]$ is associated with an update denoted by $\mathbf{y}_j^{(0)}$. Following each training round, the updates are revised according to the following rule:

$$\mathbf{y}_j^{(t+1)} = \begin{cases} \mathbf{g}_j^{(t)} & \text{if } j \in S^{(t)} \\ \mathbf{y}_j^{(t)} & \text{if } j \notin S^{(t)} \end{cases}, \text{ for all } j \in [N]. \quad (4)$$

For the quantised variant, equation (4) is modified as follows:

$$\mathbf{y}_j^{(t+1)} = \begin{cases} \text{QUANT}(\mathbf{g}_j^{(t)}) & \text{if } j \in S^{(t)} \\ \mathbf{y}_j^{(t)} & \text{if } j \notin S^{(t)} \end{cases}, \text{ for all } j \in [N]. \quad (5)$$

Equations (4) and (5), corresponding to FEDADAVR and FEDADAVR-QUANT, respectively, ensure that $\mathbf{y}_j^{(t)}$ consistently stores the most recent update for each client j , and require $\mathcal{O}(Nd)$ memory on the server.

To compute the variance-reduced model update $\mathbf{r}^{(t)}$, the received updates $\mathbf{g}_i^{(t)}$ from participating clients are jointly utilised with the stored updates $\mathbf{y}_j^{(t)}$:

$$\mathbf{r}^{(t)} = \sum_{i \in S^{(t)}} p_i (\mathbf{g}_i^{(t)} - \mathbf{y}_i^{(t)}) + \sum_{j=1}^N p_j \mathbf{y}_j^{(t)}. \quad (6)$$

For the quantised variant, equation (6) is modified as follows,

$$\mathbf{r}^{(t)} = \sum_{i \in S^{(t)}} p_i (\mathbf{g}_i^{(t)} - \mathbf{y}_i^{(t)}) + \sum_{j=1}^N p_j \text{DEQUANT}(\mathbf{y}_j^{(t)}). \quad (7)$$

Subsequently, $\mathbf{r}^{(t)}$ is employed to compute the pseudo-gradient for the adaptive optimiser using the client learning rate η_c :

$$\mathbf{G}^{(t)} = \mathbf{r}^{(t)} \eta_c. \quad (8)$$

The weight decay parameter λ in the adaptive optimiser is applied only when $\lambda \neq 0$. The update of $\mathbf{G}^{(t)}$ incorporates λ as follows:

$$\mathbf{G}^{(t)} = \mathbf{G}^{(t)} + \lambda \mathbf{w}^{(t)}. \quad (9)$$

Finally, $\mathbf{G}^{(t)}$ is used to update the global model:

$$\mathbf{w}^{(t+1)} = \mathbf{w}^{(t)} - \begin{cases} \eta_s \frac{\mathbf{G}^{(t)}}{\sqrt{z_t} + \epsilon} & \text{(Adagrad)} \\ \eta_s \frac{\hat{m}_t}{\sqrt{\hat{v}_t} + \epsilon} & \text{(Adam)} \\ \eta_s \frac{\hat{m}_t}{\sqrt{\hat{z}_t} + \epsilon} & \text{(Adabelief)} \\ \eta_s \frac{\hat{m}_t}{\sqrt{\hat{v}_t} + \epsilon} & \text{(Yogi)} \\ \eta_s r_t \hat{r}_t & \text{(Lamb)} \end{cases}. \quad (10)$$

Equation (10) presents the final parameter update of each communication round t . Each optimiser requires the current global model $\mathbf{w}^{(t)}$, the pseudo-gradient $\mathbf{G}^{(t)}$, the server learning rate η_s , and additional hyperparameters. For instance, in the Adagrad optimiser, the accumulator z_t is updated as $z_t = z_{t-1} + \mathbf{G}^{(t)} \odot \mathbf{G}^{(t)}$. This accumulator is then used to update the global model according to $\mathbf{w}^{(t+1)} = \mathbf{w}^{(t)} - \eta_s \frac{\mathbf{G}^{(t)}}{\sqrt{z_t} + \epsilon}$, where ϵ is a small constant.

To summarise Algorithm 2, the server initially transmits the current global model $\mathbf{w}^{(t)}$ to the selected clients $S^{(t)}$, who subsequently perform parallel local updates using their private datasets \mathcal{D}_n . Each participating client then returns an update $\mathbf{g}_i^{(t)}$ to the server. Upon receiving the updates, the server first computes the variance-reduced update $\mathbf{r}^{(t)}$, which is then employed to determine the server-side pseudo-gradient $\mathbf{G}^{(t)}$. This $\mathbf{G}^{(t)}$ is subsequently processed by an adaptive optimiser together with its associated parameters.

Algorithm 2 FEDADAVR and FEDADAVR-QUANT

```

1: Initialisation: Set initial model parameters  $\mathbf{w}^{(0)}$ , server learning rate  $\eta_s$ , client learning rate  $\eta_c$ , number of rounds  $T$ , and initial states  $\mathbf{y}_j^{(0)} = 0$  for all  $j \in [N]$ , with  $m_0 = 0$ ,  $v_0 = 0$ , and  $z_0 = 0$ 
2: for  $t = 0, 1, \dots, T - 1$  do
3:   Send  $\mathbf{w}^{(t)}$  to all active devices  $i \in S^{(t)}$ 
4:   // Client Side
5:   for  $i \in S^{(t)}$  do
6:      $\mathbf{g}_i^{(t)} \leftarrow \text{DEVICEUPDATE}(i, \mathbf{w}^{(t)}, \eta_c)$ 
7:   end for
8:   // Server Side
9:    $\mathbf{r}^{(t)} \leftarrow \sum_{i \in S^{(t)}} p_i (\mathbf{g}_i^{(t)} - \mathbf{y}_i^{(t)})$ 
10:   $\mathbf{G}^{(t)} \leftarrow \mathbf{r}^{(t)} \eta_c$ 
11:   $\mathbf{w}^{(t+1)} \leftarrow \begin{cases} \text{ADAGRADOPT}(\mathbf{w}^{(t)}, \mathbf{G}^{(t)}, \eta_s, z_t) \\ \text{ADAMOPT}(\mathbf{w}^{(t)}, \mathbf{G}^{(t)}, \eta_s, m_t, v_t) \\ \text{ADABELIEFOPT}(\mathbf{w}^{(t)}, \mathbf{G}^{(t)}, \eta_s, m_t, z_t) \\ \text{YOGIOPT}(\mathbf{w}^{(t)}, \mathbf{G}^{(t)}, \eta_s, m_t, v_t) \\ \text{LAMBOOPT}(\mathbf{w}^{(t)}, \mathbf{G}^{(t)}, \eta_s, m_t, v_t) \end{cases}$ 
12:  for  $j \in [N]$  do
13:     $\mathbf{y}_j^{(t+1)} \leftarrow \begin{cases} \mathbf{g}_j^{(t)} & \text{if } j \in S^{(t)} \\ \mathbf{y}_j^{(t)} & \text{if } j \notin S^{(t)} \end{cases}$ 
14:     $\mathbf{y}_j^{(t+1)} \leftarrow \begin{cases} \text{QUANT}(\mathbf{g}_j^{(t)}) & \text{if } j \in S^{(t)} \\ \mathbf{y}_j^{(t)} & \text{if } j \notin S^{(t)} \end{cases}$ 
15:  end for
16: end for

```

The optimiser then updates the global model to $\mathbf{w}^{(t+1)}$, and the server stores the most recent client updates $\mathbf{y}_j^{(t+1)}$ in memory for use in the subsequent round, considering the set of participating clients. This procedure is iterated for T communication rounds. As only the final update expression in eq. (10) is employed in this context, the corresponding modified pseudocode and formulations for the adaptive optimisers are presented in Appendix B. Algorithm 2 provides the pseudocode for the proposed methods, FEDADAVR and FEDADAVR-QUANT, which depend on several components, including the individual client update routine (Algorithm 1), the selected adaptive optimisers (Algorithms 3, 4, 5, 6, and 7) outlined in Appendix B, and the quantisation procedure for FEDADAVR-QUANT detailed in Algorithm 8 (Appendix C). For more information regarding the adaptive optimisers, the reader is referred to Adagrad (Duchi et al., 2011), Adam (Kingma & Ba, 2014), Adabelief (Zhuang et al., 2020), Yogi (Zaheer et al., 2018), and Lamb (You et al., 2020).

4.1. Comparison of Algorithms

This work relates closely to several state-of-the-art strategies. A brief comparison of these methods with the proposed algorithm is provided below:

MIFA. Authors of MIFA were among the first to utilise memory for storing the latest observed client updates in FL to address the issue of unpredictable client unavailability (Gu et al., 2021). Their aggregation procedure follows a SAG-like approach (Schmidt et al., 2013), which assigns equal weight to both the most recent and previous updates, thereby impeding convergence speed. Moreover, MIFA requires all clients to participate in the initial round, a condition rarely met in practical federated learning scenarios. In contrast, neither of the proposed algorithms relies on uniform weighting, nor do they require complete client participation at the outset.

FedVARP and ClusterFedVARP. Variance due to partial client participation is a major source of error in FL, first addressed by the authors of FedVARP (Jhunjhunwala et al., 2022). FedVARP applies a SAGA-like variance reduction technique on the server to mitigate errors from partial participation. Its variant, ClusterFedVARP, groups clients into clusters to improve memory efficiency by storing a single cluster update rather than individual updates. Although both variants outperform earlier state-of-the-art methods in highly non-IID settings, experiments show relatively slow convergence, potentially due to the fixed server learning rate (absence of server-side adaptivity). The proposed FEDADAVR adopts a similar SAGA-based reduction but replaces the fixed learning rate with an adaptive optimiser. Moreover, the calculation of $\mathbf{y}^{(t)}$, representing the latest updates for variance reduction, is redefined in FEDADAVR. According to our experiments, these refinements lead to improved performance in both IID and non-IID cases. To further enhance memory efficiency, FEDADAVR-QUANT is proposed, where the latest client updates are stored in a quantised representation.

SCAFFOLD. Designed to address client drift error, SCAFFOLD is among the earliest works to highlight this challenge (Karimireddy et al., 2020). It employs a SAGA-like technique (Defazio et al., 2014) enhanced with control variates, which necessitate communication between server and clients. While effective, these control variates increase communication overhead and slow down the overall federated learning process. In contrast, FEDADAVR requires clients to perform local SGD and transmit only local weight updates, without additional information for variance reduction. Consequently, FEDADAVR achieves lower communication costs.

FedOpt. FedOpt utilises adaptive optimisers such as Adam, Adagrad, and Yogi in federated settings (Reddi et al., 2021).

Inspired by the success of adaptive optimisers in non-federated contexts, these algorithms have demonstrated substantial performance improvements. The current work also employs these optimisers following the application of SAGA-like variance reduction. Experimental findings indicate that integrating adaptive optimisation after variance reduction further accelerates convergence. Although Adabelief and Lamb optimisers are additionally considered here, other research applying these specific optimisers directly has not been included in this study.

5. Convergence Analysis

This section presents the convergence results of the proposed algorithm, with the following assumptions introduced as a preliminary foundation.

Assumption 5.1 (Lipschitz gradient). Each local objective function f_i is assumed to be differentiable, and there exists a constant L such that, for all i , $\|\nabla f_i(\mathbf{x}) - \nabla f_i(\mathbf{y})\| \leq L \|\mathbf{x} - \mathbf{y}\|$.

Assumption 5.2 (Bounded local and global variance). The gradient computed at each client is assumed to be an unbiased estimator of the corresponding local gradient, with its variance bounded by $\mathbb{E}_{\xi_i \sim D_i} \|\nabla f_i(\mathbf{w}, \xi_i) - \nabla f_i(\mathbf{w})\|^2 \leq \sigma^2$. Additionally, it is assumed that there exists a constant $\sigma_g > 0$ such that the global gradient variance is bounded as $\|\nabla f(\mathbf{w}) - \nabla f(\mathbf{w})\|^2 \leq \sigma_g^2$, for all i .

Assumption 5.3 (Bounded gradients). The gradient of each client's objective function is assumed to be bounded; that is, for any i , it holds that $\|\nabla f_i(\mathbf{w})\| \leq G$.

Assumptions 5.1 and 5.3 are standard in the nonconvex optimisation literature, guaranteeing the L -smoothness of each local objective function and the boundedness of gradient norms, respectively. Assumption 5.2 is widely adopted in existing studies on federated optimisation. The subsequent analysis presents the convergence behaviour of FEDADAVER under the use of the Adagrad optimiser. The convergence proofs for other adaptive methods (e.g., Yogi or Adam) follow analogously.

Theorem 5.4 (Convergence of FedAdaVR). *Suppose the functions $\{f_i\}$ satisfy Assumptions 5.1, 5.2, and 5.3. In each round of FedAdaVR, the server selects a subset $|\mathcal{S}^{(t)}|=M$ of the total N clients uniformly at random to conduct K local SGD steps. If the server and client learning rates (i.e. η_s, η_c) satisfy*

$$\begin{aligned} \eta_s &\leq \min \left\{ \frac{1}{3L}, \sqrt{\frac{1}{12\epsilon L^2}} \right\}, \\ \eta_c &\leq \min \left\{ \left(\frac{\epsilon}{64AL^2K^2(K-1)G\sqrt{T}} \right)^{1/3}, \right. \\ &\quad \left. \frac{1}{8\sqrt{AL}\sqrt{K(K-1)}}, \frac{\epsilon^2}{6KG^2}, \frac{\epsilon}{4(\epsilon+2)KG\sqrt{T}} \right\}, \end{aligned}$$

then the sequence of iterates $\{\mathbf{w}^{(t)}\}$ of FedAdaVR satisfies

$$\begin{aligned} \min_{0 \leq t \leq T-1} \mathbb{E} \|\nabla f(\mathbf{w}^t)\|^2 \\ \leq \frac{4(f(\mathbf{w}^0) - f^*)}{T} + 4(A_1 \sigma_g^2 + A_2 \sigma^2 + A_3), \end{aligned}$$

where $A_1 := 4\eta_c^2 L^2 K (K-1)$,

$$A_2 := \eta_c^2 L^2 (K-1) + \frac{\eta_s}{2MK\epsilon} + \frac{\eta_s}{M\epsilon},$$

$$A_3 := \frac{\eta_s}{2\epsilon^2} \eta_c^2 K^2 M^2 G^2, \text{ and } f^* = \min_x f(x).$$

The proof of the convergence of FedAdaVR is deferred to Appendix A due to space constraints. The term $A_1 \sigma_g^2$ represents the client drift error, while $A_2 \sigma^2$ corresponds to the stochastic gradient error. In comparison with the *FedAvg Error Decomposition* theorem presented in (Jhunjhunwala et al., 2022), which demonstrates that the error of a federated learning algorithm can be decomposed into stochastic gradients, partial client participation, and client drift, it is observed that the proposed FedAdaVR eliminates the partial participation error, while preserving the client drift error $A_1 \sigma_g^2$ and the stochastic sampling error $A_2 \sigma^2$.

To derive an explicit dependence on T and K , the above result is simplified under a specific choice of η_c, η_s , and ϵ .

Corollary 5.5. *Suppose η_c and η_s are such that the conditions in Theorem 5.4 are satisfied, and also suppose $\eta_c = \Theta(1/(KL\sqrt{T}))$, $\eta_s = \Theta(KM/T)$, $\epsilon = G/L$. Then for sufficiently large T , the iterates of FedAdaVR satisfy*

$$\begin{aligned} \min_{0 \leq t \leq T-1} \mathbb{E} \|\nabla f(\mathbf{w}^t)\|^2 \leq \mathcal{O} \left(\frac{f(\mathbf{w}^0) - f^*}{T} \right) + \\ \mathcal{O} \left(\frac{\sigma_g^2}{T} + \frac{\sigma^2}{KT} + \frac{(L+LK)\sigma^2}{GT} + \frac{KM^3}{T^2} \right). \quad (11) \end{aligned}$$

6. Experiments

The experimental evaluation comprises three primary components: an overview of the experimental setup across diverse configurations (further details in Appendix D); a comparative analysis of the proposed algorithm against state-of-the-art baselines (extended analysis in Appendix F.1); and an evaluation of FEDADAVER and FEDADAVER-QUANT utilising various adaptive optimisers (additional results in Appendix F.2). Due to space constraints, the ablation study of FEDADAVER (Appendix E), details and results comparison of the quantisation methods (Appendix C and F.2.1), and the computational (Appendix F.4) and communication (Appendix F.3) comparisons against baselines are provided exclusively in the Appendix. Unless otherwise specified, all experiments utilised FP16 quantisation; due to computational constraints, a comprehensive ablation comparing FP32, FP16, Int8, and Int4 precisions was conducted exclusively on the CIFAR-10 dataset (LQ-1 partition) and is detailed in Appendix F.2.1.

6.1. Experimental Configuration

All federated learning experiments were implemented using the Flower framework (Beutel et al., 2020), with PyTorch (Paszke et al., 2019) employed for local model training. The evaluations were conducted on three computer vision datasets (MNIST, FMNIST, and CIFAR-10) and one natural language processing (NLP) dataset (Shakespeare). Vision datasets were partitioned under six distinct configurations: IID, IID-NonIID (mix of IID and non-IID), Dirichlet, LQ-1, LQ-2, and LQ-3 (Li et al., 2022b). For the Shakespeare dataset, we adopted the realistic ‘‘Natural ID’’ partitioning strategy as defined in the LEAF benchmark (Caldas et al., 2018) using Flower (Beutel et al., 2020). A concise overview of the datasets and their respective partitioning strategies is presented in Appendices D.1 and D.2.

For MNIST and FMNIST, the LeNet-5 architecture (Lecun et al., 1998) was adopted, which is a simple convolutional neural network (CNN) comprising seven layers. For CIFAR-10, the more complex ResNet-18 architecture (He et al., 2016) was employed, with batch normalisation replaced by group normalisation (Hsieh et al., 2020). For the Shakespeare dataset, we utilise a recurrent neural network (RNN) based on Gated Recurrent Units (GRU) (Chung et al., 2014). The GRU architecture consists of an 8-dimensional character embedding layer, followed by a single GRU layer with 128 hidden units, and concludes with a fully connected layer mapping the final hidden state to the character size. The MNIST and FMNIST datasets were partitioned across 500 clients, the CIFAR-10 dataset across 250 clients, and the Shakespeare dataset partitioned into 904 clients for training. In each federated learning round, five clients were selected uniformly at random, without replacement, from the complete client set. The test datasets were partitioned identically to the training distributions. For the vision datasets, 250 clients were sampled for evaluation after each round, whereas for the Shakespeare dataset, the model was evaluated on a held-out set of 225 previously separated clients of 1129 (904 clients for training).

Hyperparameter configurations were tailored to each specific algorithm to ensure fair benchmarking. All experiments were executed using a fixed random seed (42) for reproducibility. For client-side optimisation, we performed a grid search over the learning rate $\eta_c \in \{0.001, 0.01, 0.1\}$ and report the results of the best-performing configuration. For methods incorporating server-side optimisation (FedVARP, FEDADAVR, and FEDADAVR-QUANT), we conducted an additional grid search to determine the optimal server learning rate η_s . Specifically, we explored $\eta_s \in \{0.01, 0.1, 1.0\}$ for FedVARP, and $\eta_s \in \{0.001, 0.005, 0.01\}$ for the FEDADAVR variants. The best-performing models for FedVARP, FEDADAVR, and FEDADAVR-QUANT across datasets and partitioning strategies are summarised in Tables 6, 7, 8, and

9 in Appendix F.2.

As FEDADAVR and FEDADAVR-QUANT incorporate adaptive optimisers, additional hyperparameters were necessary. A comprehensive overview of the parameters and hyperparameters utilised in the experiments is presented in Table 1 (Appendix D.3). The total number of training rounds and the specific rounds used for computing the average accuracy, based on the dataset and its partitioning strategy, are outlined in Table 2 (Appendix D.3). In each case, the average accuracy was computed over a predefined subset of the final training rounds.

6.2. Comparison with State-of-the-Art Methods

To evaluate the proposed algorithms against state-of-the-art methods, we compared them with the most relevant baselines: FedAvg (McMahan et al., 2017), FedProx (Li et al., 2020b), SCAFFOLD (Karimireddy et al., 2020), FedNova (Wang et al., 2020), FedAdam (Reddi et al., 2021), FedAdagrad (Reddi et al., 2021), FedYogi (Reddi et al., 2021), MIFA (Gu et al., 2021), and FedVARP (Jhunjhunwala et al., 2022). Accuracy and training loss served as the primary metrics for performance assessment. Figure 1 illustrates the accuracy trajectories, while Figure 3 in Appendix F.1 presents the corresponding loss curves across the varying data partitioning strategies and vision datasets. Figure 4 in Appendix F.1.7 illustrates the results on the Shakespeare dataset.

FEDADAVR consistently outperforms all baseline algorithms in nearly all scenarios, despite incurring no additional communication or computational overhead at the clients. The experimental setup posed significant challenges (variance and data heterogeneity), particularly under the LQ-1 partitioning scheme (where each client holds data from only one class) and with very limited client participation rates (1% for MNIST and FMNIST, 2% for CIFAR-10 and, < 1% for Shakespeare). This setting renders learning especially difficult for all algorithms. In LQ-1, data are sorted by label and partitioned into a single chunk (two chunks for LQ-2 and three for LQ-3), such that each partition contains data from only one (or two or three) class(es).

FedAdam failed to cope with this exceptionally demanding scenario on MNIST and FMNIST datasets and also underperformed in IID data distributions combined with extreme partial client participation. While the other baseline methods remained functional, both FEDADAVR and its quantised variant, FEDADAVR-QUANT, demonstrated superior performance. FedYogi exhibited strong results throughout the experiments, which was somewhat unexpected given the low client participation rates, indicating its capacity to handle partial client participation errors. Although FedVARP outperformed other baselines under the highly challenging LQ-1 data partitioning on the CIFAR-10 dataset—exhibiting

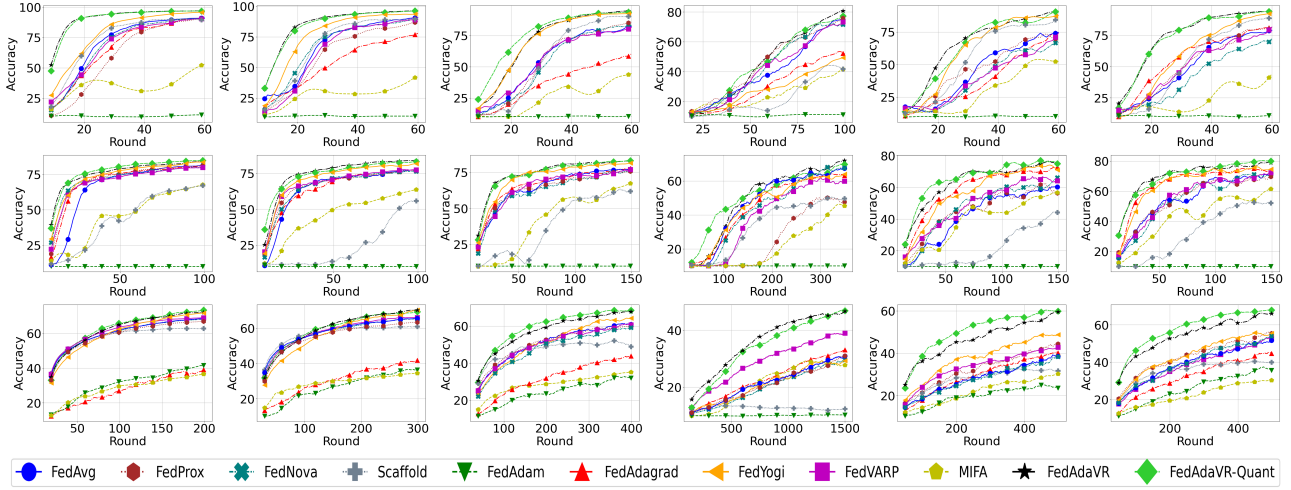


Figure 1. Accuracy Comparison Across Various Data Partitioning Methods—IID, IID-NonIID, Dirichlet, LQ-1, LQ-2, and LQ-3 (Left to Right)—on MNIST (Top), FMNIST (Middle), and CIFAR-10 (Bottom) Datasets.

improved robustness to partial client participation error—it still falls significantly short of the performance achieved by our proposed algorithms. MIFA also achieved reasonable performance but suffered from slower convergence. Similarly, FedAvg, FedAdagrad, FedProx, SCAFFOLD, and FedNova displayed sluggish convergence rates. While FedAdagrad remains a strong competitor in the NLP domain (Shakespeare), our method matches its performance there while strictly outperforming it in vision tasks, thereby establishing a broader cross-domain superiority.

6.3. Comparison of Experimental Results Between FEDADAVER and FedAdaVR-Quant Using Various Adaptive Optimisers

Both algorithms exhibit rapid convergence and comparable performance. Despite storing previous local model weights in a quantised format, FEDADAVER-QUANT maintains similar accuracy while offering enhanced memory efficiency. This observation suggests that FL algorithms employing memory to retain historical updates for global aggregation are only marginally impacted by quantisation. This minimal changes arises from the negligible difference between client weights pre- and post-quantisation. When computing $\mathbf{y}^{(t)}$, quantisation errors are randomly distributed, leading to an inconsequential deviation that does not materially affect the performance of the FL algorithm. Therefore, our quantised version sometimes perform better than non-quantised version.

Both FEDADAVER and FEDADAVER-QUANT employ adaptive optimisers. Tables 6, 7, 8, and 9 detail the accuracy achieved under various optimiser and server learning rate. These tables present average accuracy over the final training rounds, as detailed in Table 2. The best accuracy values and

configurations for both algorithms, as recorded in Tables 6, 7, 8, and 9, are illustrated in Figures 1, 3 and 4. Discussion regarding server learning rates and optimiser selection is provided in Appendix F.2.2.

7. Conclusion and Future Work

This study introduces a novel FL algorithm, FEDADAVER, which integrates an adaptive optimiser with variance reduction mechanisms. Extensive experiments demonstrate that this approach significantly enhances convergence speed while mitigating the variance introduced by partial client participation. The algorithm leverages server-side memory to retain the most recent client updates, thereby emulating continuous client availability during aggregation. We also present convergence results of FEDADAVER and prove that our proposed algorithm can eliminate partial client participation error. To further optimise memory efficiency, we propose a quantised variant, FEDADAVER-QUANT, wherein updates are stored in FP16, Int8, or Int4 formats, thereby reducing memory requirements by up to 87.5%.

Limitations and Future Work. While FEDADAVER and FEDADAVER-QUANT consistently outperform state-of-the-art baselines, our current study focuses on three deterministic linear quantisation schemes. Future work will explore advanced compression techniques, such as non-linear or vector quantisation, to unlock further efficiency gains, alongside evaluations on a broader spectrum of model architectures and datasets. Additionally, we acknowledge that fair benchmarking in federated learning is challenging due to the high dimensionality of the hyperparameter space. Although we conducted extensive grid searches to ensure robust comparisons, further performance improvements might be attainable for all methods through more hyperparameter tuning.

Acknowledgements

The work has been partially supported by the SLAIDER project funded by the UK Research and Innovation Grant EP/Y018281/1. This research used the ALICE High Performance Computing facility at the University of Leicester.

References

Abdelmoniem, A. M. and Canini, M. Towards mitigating device heterogeneity in federated learning via adaptive model quantization. In *Proceedings of the 1st Workshop on Machine Learning and Systems*, EuroSys '21. ACM, April 2021. doi: 10.1145/3437984.3458839.

Batardière, B. and Kwon, J. Finite-sum optimization: Adaptivity to smoothness and loopless variance reduction, 2023.

Beutel, D. J., Topal, T., Mathur, A., Qiu, X., Fernandez-Marques, J., Gao, Y., Sani, L., Li, K. H., Parcollet, T., de Gusmão, P. P. B., and Lane, N. D. Flower: A friendly federated learning research framework, 2020.

Caldas, S., Duddu, S. M. K., Wu, P., Li, T., Konečný, J., McMahan, H. B., Smith, V., and Talwalkar, A. Leaf: A benchmark for federated settings, 2018.

Chen, S., Li, L., Wang, G., Pang, M., and Shen, C. Federated learning with heterogeneous quantization bit allocation and aggregation for internet of things. *IEEE Internet of Things Journal*, 11(2):3132–3143, January 2024. ISSN 2372-2541. doi: 10.1109/jiot.2023.3296493.

Chen, X., Li, X., and Li, P. Toward communication efficient adaptive gradient method. In *Proceedings of the 2020 ACM-IMS on Foundations of Data Science Conference*, FODS '20, pp. 119–128, New York, NY, USA, 2020. Association for Computing Machinery. ISBN 9781450381031. doi: 10.1145/3412815.3416891.

Chung, J., Gulcehre, C., Cho, K., and Bengio, Y. Empirical evaluation of gated recurrent neural networks on sequence modeling, 2014.

Defazio, A., Bach, F., and Lacoste-Julien, S. Saga: a fast incremental gradient method with support for non-strongly convex composite objectives. In *Proceedings of the 28th International Conference on Neural Information Processing Systems - Volume 1*, NIPS'14, pp. 1646–1654, Cambridge, MA, USA, 2014. MIT Press.

Deng, L. The mnist database of handwritten digit images for machine learning research. *IEEE Signal Processing Magazine*, 29(6):141–142, 2012.

Duchi, J., Hazan, E., and Singer, Y. Adaptive subgradient methods for online learning and stochastic optimization. *Journal of Machine Learning Research*, 12(61): 2121–2159, 2011.

Gu, X., Huang, K., Zhang, J., and Huang, L. Fast federated learning in the presence of arbitrary device unavailability. In *Proceedings of the 35th International Conference on Neural Information Processing Systems*, NIPS '21, Red Hook, NY, USA, 2021. Curran Associates Inc. ISBN 9781713845393.

Guendouzi, B. S., Ouchani, S., EL Assaad, H., and EL Zacher, M. A systematic review of federated learning: Challenges, aggregation methods, and development tools. *Journal of Network and Computer Applications*, 220: 103714, November 2023. ISSN 1084-8045. doi: 10.1016/j.jnca.2023.103714.

Gupta, K., Fournarakis, M., Reisser, M., Louizos, C., and Nagel, M. Quantization robust federated learning for efficient inference on heterogeneous devices. *Transactions on Machine Learning Research*, 2023. ISSN 2835-8856.

He, K., Zhang, X., Ren, S., and Sun, J. Deep residual learning for image recognition. In *Proceedings of the IEEE conference on computer vision and pattern recognition*, pp. 770–778, 2016.

Howard, A., Sandler, M., Chen, B., Wang, W., Chen, L.-C., Tan, M., Chu, G., Vasudevan, V., Zhu, Y., Pang, R., Adam, H., and Le, Q. Searching for mobilenetv3. In *2019 IEEE/CVF International Conference on Computer Vision (ICCV)*, pp. 1314–1324. IEEE, October 2019. doi: 10.1109/iccv.2019.00140.

Howard, A. G., Zhu, M., Chen, B., Kalenichenko, D., Wang, W., Weyand, T., Andreetto, M., and Adam, H. Mobilenets: Efficient convolutional neural networks for mobile vision applications, 2017.

Hsieh, K., Phanishayee, A., Mutlu, O., and Gibbons, P. B. The non-iid data quagmire of decentralized machine learning. In *Proceedings of the 37th International Conference on Machine Learning*, ICML'20. JMLR.org, 2020.

Iandola, F. N., Han, S., Moskewicz, M. W., Ashraf, K., Dally, W. J., and Keutzer, K. SqueezeNet: Alexnet-level accuracy with 50x fewer parameters and <0.5mb model size, 2016.

Jhunjhunwala, D., Sharma, P., Nagarkatti, A., and Joshi, G. Fedvarp: Tackling the variance due to partial client participation in federated learning. In Cussens, J. and Zhang, K. (eds.), *Proceedings of the Thirty-Eighth Conference on Uncertainty in Artificial Intelligence*, volume 180 of *Proceedings of Machine Learning Research*, pp. 906–916. PMLR, 01–05 Aug 2022.

Johnson, R. and Zhang, T. Accelerating stochastic gradient descent using predictive variance reduction. In Burges, C., Bottou, L., Welling, M., Ghahramani, Z., and Weinberger, K. (eds.), *Advances in Neural Information Processing Systems*, volume 26. Curran Associates, Inc., 2013.

Kairouz, P., McMahan, H. B., Avent, B., Bellet, A., Benois, M., Bhagoji, A. N., Bonawitz, K., Charles, Z., Cormode, G., Cummings, R., D’Oliveira, R. G. L., Eichner, H., Rouayheb, S. E., Evans, D., Gardner, J., Garrett, Z., Gascón, A., Ghazi, B., Gibbons, P. B., Gruteser, M., Harchaoui, Z., He, C., He, L., Huo, Z., Hutchinson, B., Hsu, J., Jaggi, M., Javidi, T., Joshi, G., Khodak, M., Konečný, J., Korolova, A., Koushanfar, F., Koyejo, S., Lepoint, T., Liu, Y., Mittal, P., Mohri, M., Nock, R., Özgür, A., Pagh, R., Raykova, M., Qi, H., Ramage, D., Raskar, R., Song, D., Song, W., Stich, S. U., Sun, Z., Suresh, A. T., Tramèr, F., Vepakomma, P., Wang, J., Xiong, L., Xu, Z., Yang, Q., Yu, F. X., Yu, H., and Zhao, S. Advances and open problems in federated learning, 2019.

Kao, C.-H. and Wang, Y.-C. F. Fedbug: A bottom-up gradual unfreezing framework for federated learning, 2023.

Karimi, B., Li, P., and Li, X. Fed-LAMB: Layer-wise and dimension-wise locally adaptive federated learning. In Evans, R. J. and Shpitser, I. (eds.), *Proceedings of the Thirty-Ninth Conference on Uncertainty in Artificial Intelligence*, volume 216 of *Proceedings of Machine Learning Research*, pp. 1037–1046. PMLR, 31 Jul–04 Aug 2023.

Karimireddy, S. P., Kale, S., Mohri, M., Reddi, S., Stich, S., and Suresh, A. T. SCAFFOLD: Stochastic controlled averaging for federated learning. In III, H. D. and Singh, A. (eds.), *Proceedings of the 37th International Conference on Machine Learning*, volume 119 of *Proceedings of Machine Learning Research*, pp. 5132–5143. PMLR, 13–18 Jul 2020.

Khaled, A., Mishchenko, K., and Richtarik, P. Tighter theory for local sgd on identical and heterogeneous data. In Chiappa, S. and Calandra, R. (eds.), *Proceedings of the Twenty Third International Conference on Artificial Intelligence and Statistics*, volume 108 of *Proceedings of Machine Learning Research*, pp. 4519–4529. PMLR, 26–28 Aug 2020.

Kingma, D. P. and Ba, J. Adam: A method for stochastic optimization, 2014.

Krishnamoorthi, R. Quantizing deep convolutional networks for efficient inference: A whitepaper, 2018.

Krizhevsky, A. Learning multiple layers of features from tiny images. Technical report, University of Toronto, 2009.

Lecun, Y., Bottou, L., Bengio, Y., and Haffner, P. Gradient-based learning applied to document recognition. *Proceedings of the IEEE*, 86(11):2278–2324, 1998. doi: 10.1109/5.726791.

Li, C., Li, G., and Varshney, P. K. Decentralized federated learning via mutual knowledge transfer. *IEEE Internet of Things Journal*, 9(2):1136–1147, 2022a. doi: 10.1109/JIOT.2021.3078543.

Li, Q., Diao, Y., Chen, Q., and He, B. Federated learning on non-iid data silos: An experimental study. In 2022 IEEE 38th International Conference on Data Engineering (ICDE), pp. 965–978, 2022b. doi: 10.1109/ICDE53745.2022.00077.

Li, T., Sahu, A. K., Talwalkar, A., and Smith, V. Federated learning: Challenges, methods, and future directions. *IEEE Signal Processing Magazine*, 37(3):50–60, may 2020a. doi: 10.1109/msp.2020.2975749.

Li, T., Sahu, A. K., Zaheer, M., Sanjabi, M., Talwalkar, A., and Smith, V. Federated optimization in heterogeneous networks. In Dhillon, I., Papailiopoulos, D., and Sze, V. (eds.), *Proceedings of Machine Learning and Systems*, volume 2, pp. 429–450, 2020b.

Li, X., Huang, K., Yang, W., Wang, S., and Zhang, Z. On the convergence of fedavg on non-iid data. In *International Conference on Learning Representations*, 2020c.

Liu, Z., Mao, H., Wu, C.-Y., Feichtenhofer, C., Darrell, T., and Xie, S. A convnet for the 2020s. *Proceedings of the IEEE/CVF Conference on Computer Vision and Pattern Recognition (CVPR)*, 2022.

Ma, N., Zhang, X., Zheng, H.-T., and Sun, J. *ShuffleNet V2: Practical Guidelines for Efficient CNN Architecture Design*, pp. 122–138. Springer International Publishing, 2018. ISBN 9783030012649. doi: 10.1007/978-3-030-01264-9_8.

Mansour, A. B., Carenini, G., and Duplessis, A. Tackling computational heterogeneity in fl: A few theoretical insights, 2023.

Mao, Y., Zhao, Z., Yan, G., Liu, Y., Lan, T., Song, L., and Ding, W. Communication-efficient federated learning with adaptive quantization. *ACM Transactions on Intelligent Systems and Technology*, 13(4):1–26, aug 2022. doi: 10.1145/3510587.

McMahan, B., Moore, E., Ramage, D., Hampson, S., and Arcas, B. A. y. Communication-Efficient Learning of Deep Networks from Decentralized Data. In Singh, A. and Zhu, J. (eds.), *Proceedings of the 20th International Conference on Artificial Intelligence and Statistics*, volume 54 of *Proceedings of Machine Learning Research*, pp. 1273–1282. PMLR, 20–22 Apr 2017.

Nguyen, L. M., Liu, J., Scheinberg, K., and Takáč, M. Sarah: a novel method for machine learning problems using stochastic recursive gradient. In *Proceedings of the 34th International Conference on Machine Learning - Volume 70*, ICML'17, pp. 2613–2621. JMLR.org, 2017.

Paszke, A., Gross, S., Massa, F., Lerer, A., Bradbury, J., Chanan, G., Killeen, T., Lin, Z., Gimelshein, N., Antiga, L., Desmaison, A., Kopf, A., Yang, E., DeVito, Z., Raison, M., Tejani, A., Chilamkurthy, S., Steiner, B., Fang, L., Bai, J., and Chintala, S. Pytorch: An imperative style, high-performance deep learning library. In Wallach, H., Larochelle, H., Beygelzimer, A., d'Alché-Buc, F., Fox, E., and Garnett, R. (eds.), *Advances in Neural Information Processing Systems*, volume 32. Curran Associates, Inc., 2019.

Rahman, K. M. J., Ahmed, F., Akhter, N., Hasan, M., Amin, R., Aziz, K. E., Islam, A. K. M. M., Mukta, M. S. H., and Islam, A. K. M. N. Challenges, applications and design aspects of federated learning: A survey. *IEEE Access*, 9:124682–124700, 2021. ISSN 2169-3536. doi: 10.1109/access.2021.3111118.

Reddi, S. J., Kale, S., and Kumar, S. On the convergence of adam and beyond. In *International Conference on Learning Representations*, 2018.

Reddi, S. J., Charles, Z., Zaheer, M., Garrett, Z., Rush, K., Konečný, J., Kumar, S., and McMahan, H. B. Adaptive federated optimization. In *International Conference on Learning Representations*, 2021.

Reisizadeh, A., Mokhtari, A., Hassani, H., Jadbabaie, A., and Pedarsani, R. Fedpaq: A communication-efficient federated learning method with periodic averaging and quantization. In *International conference on artificial intelligence and statistics*, pp. 2021–2031. PMLR, 2020.

Ren, Y., Cao, Y., Ye, C., and Cheng, X. Two-layer accumulated quantized compression for communication-efficient federated learning: TLAQC. *Scientific Reports*, 13(1), jul 2023. doi: 10.1038/s41598-023-38916-x.

Sandler, M., Howard, A., Zhu, M., Zhmoginov, A., and Chen, L.-C. Mobilenetv2: Inverted residuals and linear bottlenecks. In *2018 IEEE/CVF Conference on Computer Vision and Pattern Recognition*, pp. 4510–4520. IEEE, June 2018. doi: 10.1109/cvpr.2018.00474.

Schmidt, M., Roux, N. L., and Bach, F. Minimizing finite sums with the stochastic average gradient, 2013.

Su, L., Xiang, M., Xu, J., and Yang, P. Federated Learning in the Presence of Adversarial Client Unavailability. *arXiv e-prints*, art. arXiv:2305.19971, May 2023. doi: 10.48550/arXiv.2305.19971.

Szegedy, C., Liu, W., Jia, Y., Sermanet, P., Reed, S., Anguelov, D., Erhan, D., Vanhoucke, V., and Rabinovich, A. Going deeper with convolutions. In *2015 IEEE Conference on Computer Vision and Pattern Recognition (CVPR)*, pp. 1–9. IEEE, June 2015. doi: 10.1109/cvpr.2015.7298594.

Tan, M. and Le, Q. EfficientNet: Rethinking model scaling for convolutional neural networks. In Chaudhuri, K. and Salakhutdinov, R. (eds.), *Proceedings of the 36th International Conference on Machine Learning*, volume 97 of *Proceedings of Machine Learning Research*, pp. 6105–6114. PMLR, 09–15 Jun 2019.

Tan, M., Chen, B., Pang, R., Vasudevan, V., Sandler, M., Howard, A., and Le, Q. V. Mnasnet: Platform-aware neural architecture search for mobile, 2018.

Varno, F., Saghayi, M., Rafiee Sevyeri, L., Gupta, S., Matwin, S., and Havaei, M. Adabest: Minimizing client drift in federated learning via adaptive bias estimation. In *Computer Vision – ECCV 2022: 17th European Conference, Tel Aviv, Israel, October 23–27, 2022, Proceedings, Part XXIII*, pp. 710–726, Berlin, Heidelberg, 2022. Springer-Verlag. ISBN 978-3-031-20049-6. doi: 10.1007/978-3-031-20050-2_41.

Wang, J. and Joshi, G. Adaptive communication strategies to achieve the best error-runtime trade-off in local-update sgd. In Talwalkar, A., Smith, V., and Zaharia, M. (eds.), *Proceedings of Machine Learning and Systems*, volume 1, pp. 212–229, 2019.

Wang, J., Liu, Q., Liang, H., Joshi, G., and Poor, H. V. Tackling the objective inconsistency problem in heterogeneous federated optimization. In *Proceedings of the 34th International Conference on Neural Information Processing Systems*, NIPS '20, Red Hook, NY, USA, 2020. Curran Associates Inc. ISBN 9781713829546.

Wang, L., Guo, Y., Lin, T., and Tang, X. Delta: diverse client sampling for fast federated learning. In *Proceedings of the 37th International Conference on Neural Information Processing Systems*, NIPS '23, Red Hook, NY, USA, 2023. Curran Associates Inc.

Warnat-Herresthal, S., Schultze, H., Shastry, K. L., Manamohan, S., Mukherjee, S., Garg, V., Sarveswara, R., Händler, K., Pickkers, P., Aziz, N. A., et al. Swarm learning for decentralized and confidential clinical machine learning. *Nature*, 594(7862):265–270, 2021.

Wen, J., Zhang, Z., Lan, Y., Cui, Z., Cai, J., and Zhang, W. A survey on federated learning: challenges and applications. *International Journal of Machine Learning and Cybernetics*, 14(2):513–535, November 2022. ISSN 1868-808X. doi: 10.1007/s13042-022-01647-y.

Xiao, H., Rasul, K., and Vollgraf, R. Fashion-mnist: a novel image dataset for benchmarking machine learning algorithms, 2017.

You, Y., Li, J., Reddi, S., Hseu, J., Kumar, S., Bhojanapalli, S., Song, X., Demmel, J., Keutzer, K., and Hsieh, C.-J. Large batch optimization for deep learning: Training bert in 76 minutes. In *International Conference on Learning Representations*, 2020.

Zaheer, M., Reddi, S., Sachan, D., and Kale, S. Adaptive methods for nonconvex optimization. In Bengio, S., Wallach, H., Larochelle, H., Grauman, K., Cesa-Bianchi, N., and Garnett, R. (eds.), *Advances in Neural Information Processing Systems*, volume 31. Curran Associates, Inc., 2018.

Zhou, S., Wu, Y., Ni, Z., Zhou, X., Wen, H., and Zou, Y. Dorefa-net: Training low bitwidth convolutional neural networks with low bitwidth gradients, 2016.

Zhuang, J., Tang, T., Ding, Y., Tatikonda, S. C., Dvornek, N., Papademetris, X., and Duncan, J. Adabelief optimizer: Adapting stepsizes by the belief in observed gradients. In Larochelle, H., Ranzato, M., Hadsell, R., Balcan, M., and Lin, H. (eds.), *Advances in Neural Information Processing Systems*, volume 33, pp. 18795–18806. Curran Associates, Inc., 2020.

A. Convergence Analysis for FEDADAVER

This appendix presents the detailed convergence proof of the proposed FEDADAVER.

A.1. Basic Notations

Let $\mathcal{S}^{(t)}$ be the subset of clients sampled in round t , and let $\xi^{(t)}$ denote the stochastic randomness at round t .

$$\begin{aligned}\Delta_i^{(t)} &= \frac{1}{K} \sum_{k=0}^{K-1} \nabla f_i(\mathbf{w}_i^{(t,k)}, \xi_i^{(t,k)}), \\ h_i^{(t)} &= \frac{1}{K} \sum_{k=0}^{K-1} \nabla f_i(\mathbf{w}_i^{(t,k)}), \\ \bar{h}^{(t)} &= \frac{1}{N} \sum_{i=1}^N h_i^{(t)}, \\ \mathbf{w}^{(t+1)} &= \mathbf{w}^{(t)} - \tilde{\eta}_s \frac{1}{M} \sum_{i \in \mathcal{S}^{(t)}} \Delta_i^{(t)}, \quad \tilde{\eta}_s = \eta_s \eta_c K.\end{aligned}$$

A.2. Auxiliary Lemmas

Lemma A.1 (Young's inequality). *Given two vectors of the same dimension $\mathbf{u}, \mathbf{v} \in \mathbb{R}^d$, for every constant $\gamma > 0$ the Euclidean inner product can be bounded as*

$$\langle \mathbf{u}, \mathbf{v} \rangle \leq \frac{\|\mathbf{u}\|^2}{2\gamma} + \frac{\gamma \|\mathbf{v}\|^2}{2}.$$

Lemma A.2 (Jensen's inequality). *Given a convex function f and a random variable X , the following holds:*

$$f(\mathbb{E}[X]) \leq \mathbb{E}[f(X)].$$

Lemma A.3 (Sum of squares). *For a positive integer K and vectors $\mathbf{x}_1, \dots, \mathbf{x}_K \in \mathbb{R}^d$, the following holds:*

$$\left\| \sum_{k=1}^K \mathbf{x}_k \right\|^2 \leq K \sum_{k=1}^K \|\mathbf{x}_k\|^2.$$

Lemma A.4 (Variance under uniform, without-replacement sampling). *Let $\bar{x} = \frac{1}{N} \sum_{i=1}^N x_i$. If \bar{x} is approximated using a mini-batch \mathcal{M} of size M , sampled uniformly at random without replacement, then*

$$\mathbb{E}\left[\frac{1}{M} \sum_{i \in \mathcal{M}} x_i\right] = \bar{x},$$

and

$$\mathbb{E}\left\| \frac{1}{M} \sum_{i \in \mathcal{M}} x_i - \bar{x} \right\|^2 = \frac{1}{M} \frac{N-M}{N-1} \frac{1}{N} \sum_{i=1}^N \|x_i - \bar{x}\|^2.$$

Lemma A.5. *Suppose the function f satisfies Assumption 5.1, and that the stochastic oracles at the clients adhere to Assumptions 5.2 and 5.3. Moreover, let the client learning rate η_c be chosen such that $\eta_c \leq \frac{1}{2LK}$. Under these conditions, the iterates $\{\mathbf{w}^{(t)}\}_t$ generated by FedAdaVR satisfy*

$$\begin{aligned}\mathbb{E}_{\xi^{(t)}} \|\nabla f(\mathbf{w}^{(t)}) - \bar{\mathbf{h}}^{(t)}\|^2 &\leq \frac{1}{N} \sum_{i=1}^N \mathbb{E}_{\xi^{(t)}} \|\nabla f_i(\mathbf{w}^{(t)}) - \mathbf{h}_i^{(t)}\|^2 \\ &\leq 2\eta_c^2 L^2 (K-1) \sigma^2 + 8\eta_c^2 L^2 K (K-1) \left[\sigma_g^2 + \|\nabla f(\mathbf{w}^{(t)})\|^2 \right].\end{aligned}$$

Lemma A.6. Suppose the function f satisfies Assumption 5.1, and the stochastic oracles at the clients fulfil Assumption 5.2. Then the iterates $\{\mathbf{w}^{(t)}\}_t$ generated by FedAdaVR satisfy

$$\begin{aligned} & \mathbb{E}_{S^{(t)}, \xi^{(t)}} \|\mathbf{G}^{(t)} - \bar{\mathbf{h}}^{(t)}\|^2 \\ & \leq \frac{\sigma^2}{MK} + \frac{4(N-M)}{M(N-1)} \left[\frac{1}{N} \sum_{i=1}^N \mathbb{E}_{\xi^{(t)}} \|\mathbf{h}_i^{(t)} - \nabla f_i(\mathbf{w}^{(t)})\|^2 + \tilde{\eta}_s^2 L^2 \|\mathbf{G}^{(t-1)}\|^2 \right] + \frac{2(N-M)}{M(N-1)} \frac{1}{N} \sum_{i=1}^N \|\nabla f_i(\mathbf{w}^{(t-1)}) - \mathbf{y}_i^{(t)}\|^2. \end{aligned}$$

Lemma A.7. Suppose the function f satisfies Assumption 5.1, and the stochastic oracles at the clients comply with Assumptions 5.2 and 5.3. Then, for any $\beta > 0$, the iterates $\{\mathbf{w}^{(t)}\}_t$ generated by FedAdaVR satisfy

$$\begin{aligned} & \mathbb{E}_{S^{(t)}, \xi^{(t)}} \left[\frac{1}{N} \sum_{j=1}^N \|\nabla f_j(\mathbf{w}^{(t)}) - \mathbf{y}_j^{(t+1)}\|^2 \right] \\ & \leq \frac{M}{N} \left[\frac{\sigma^2}{K} + \frac{1}{N} \sum_{j=1}^N \mathbb{E}_{\xi^{(t)}} \|\nabla f_j(\mathbf{w}^{(t)}) - \mathbf{h}_j^{(t)}\|^2 \right] \\ & \quad + \left(1 - \frac{M}{N}\right) \left[\left(1 + \frac{1}{\beta}\right) \tilde{\eta}_s^2 L^2 \|\mathbf{G}^{(t-1)}\|^2 + (1 + \beta) \frac{1}{N} \sum_{j=1}^N \|\nabla f_j(\mathbf{w}^{(t-1)}) - \mathbf{y}_j^{(t)}\|^2 \right]. \end{aligned}$$

Lemmas A.1–A.4 are standard in proof of convergence. Our proof is inspired by (Jhunjhunwala et al., 2022). Lemmas A.5, A.6, and A.7 follow analogous statements and admit similar arguments. We therefore omit proofs for brevity.

A.3. Proof of the Theorem

Proof. Recall that the server update in FedAdaVR, based on the Adagrad optimiser, is given by:

$$\mathbf{w}^{t+1} = \mathbf{w}^t - \eta_s \frac{\mathbf{G}^{(t)}}{\sqrt{z_t} + \epsilon}.$$

As the function is L -smooth, the following inequality holds:

$$\begin{aligned} f(\mathbf{w}^{t+1}) & \leq f(\mathbf{w}^t) + \langle \nabla f(\mathbf{w}^t), \mathbf{w}^{t+1} - \mathbf{w}^t \rangle + \frac{L}{2} \|\mathbf{w}^{t+1} - \mathbf{w}^t\|^2 \\ & = f(\mathbf{w}^t) - \eta_s \langle \nabla f(\mathbf{w}^t), \frac{\mathbf{G}^{(t)}}{\sqrt{z_t} + \epsilon} \rangle + \frac{L}{2} \eta_s^2 \frac{\mathbf{G}^{(t)} \cdot \mathbf{G}^{(t)}}{(\sqrt{z_t} + \epsilon)^2}. \end{aligned}$$

Taking the expectation of $f(\mathbf{w}^{t+1})$ in the inequality above yields:

$$\begin{aligned} \mathbb{E}[f(\mathbf{w}^{t+1})] & \leq f(\mathbf{w}^t) - \eta_s \left\langle \nabla f(\mathbf{w}^t), \mathbb{E}\left[\frac{\mathbf{G}^{(t)}}{\sqrt{z_t} + \epsilon}\right] \right\rangle + \frac{\eta_s^2 L}{2} \frac{\mathbf{G}^{(t)} \cdot \mathbf{G}^{(t)}}{(\sqrt{z_t} + \epsilon)^2} \\ & = f(\mathbf{w}^t) - \eta_s \left\langle \nabla f(\mathbf{w}^t), \mathbb{E}\left[\frac{\mathbf{G}^{(t)}}{\sqrt{z_t} + \epsilon} - \frac{\mathbf{G}^{(t)}}{\sqrt{z_{t-1}} + \epsilon}\right] \right\rangle - \eta_s \left\langle \nabla f(\mathbf{w}^t), \mathbb{E}\left[\frac{\mathbf{G}^{(t)}}{\sqrt{z_{t-1}} + \epsilon}\right] \right\rangle + \frac{\eta_s^2 L}{2} \frac{\mathbf{G}^{(t)} \cdot \mathbf{G}^{(t)}}{(\sqrt{z_t} + \epsilon)^2} \\ & \leq f(\mathbf{w}^t) + \eta_s \underbrace{\left\langle \nabla f(\mathbf{w}^t), \mathbb{E}\left[-\frac{\mathbf{G}^{(t)}}{\sqrt{z_{t-1}} + \epsilon}\right] \right\rangle}_{T_1} + \eta_s \underbrace{\left\langle \nabla f(\mathbf{w}^t), \mathbb{E}\left[\frac{\mathbf{G}^{(t)}}{\sqrt{z_{t-1}} + \epsilon} - \frac{\mathbf{G}^{(t)}}{\sqrt{z_t} + \epsilon}\right] \right\rangle}_{T_2} + \frac{\eta_s^2 L}{2\epsilon^2} \mathbf{G}^{(t)} \cdot \mathbf{G}^{(t)}. \end{aligned}$$

We will first bound T_2 :

$$\begin{aligned}
 T_2 &= \left\langle \nabla f(\mathbf{w}^t), \mathbb{E} \left[\frac{\mathbf{G}^{(t)}}{\sqrt{z_{t-1}} + \epsilon} - \frac{\mathbf{G}^{(t)}}{\sqrt{z_t} + \epsilon} \right] \right\rangle \\
 &= \left\langle \nabla f(\mathbf{w}^t), \mathbb{E} \left[\frac{\mathbf{G}^{(t)}(\sqrt{z_t} - \sqrt{z_{t-1}})}{(\sqrt{z_{t,j}} + \epsilon)(\sqrt{z_{t-1,j}} + \epsilon)} \right] \right\rangle \\
 &= \mathbb{E}_{\xi^{(t)}, \mathcal{S}^{(t)}} \nabla f(\mathbf{w}^t) \cdot \mathbf{G}_i^{(t)} \cdot \left[\frac{(\sqrt{z_t} - \sqrt{z_{t-1}})}{(\sqrt{z_{t,i}} + \epsilon)(\sqrt{z_{t-1,i}} + \epsilon)} \right].
 \end{aligned}$$

Recall $z_t = z_{t-1} + \mathbf{G}^{(t)2}$ so $\mathbf{G}^{(t)2} = (\sqrt{z_t} - \sqrt{z_{t-1}})(\sqrt{z_t} + \sqrt{z_{t-1}})$. Then we have

$$\begin{aligned}
 T_2 &= \mathbb{E}_{\xi^{(t)}, \mathcal{S}^{(t)}} \nabla f(\mathbf{w}^t) \cdot \mathbf{G}_i^{(t)} \cdot \left[\frac{(\sqrt{z_t} - \sqrt{z_{t-1}})}{(\sqrt{z_{t,i}} + \epsilon)(\sqrt{z_{t-1,i}} + \epsilon)} \right] \\
 &= \mathbb{E}_{\xi^{(t)}, \mathcal{S}^{(t)}} \nabla f(\mathbf{w}^t) \\
 &\quad \cdot \mathbf{G}_i^{(t)} \left[\frac{\mathbf{G}^{(t)2}}{(\sqrt{z_t} + \epsilon)(\sqrt{z_{t-1}} + \epsilon)(\sqrt{z_t} + \sqrt{z_{t-1}})} \right] \\
 &= \mathbb{E}_{\xi^{(t)}, \mathcal{S}^{(t)}} \nabla f(\mathbf{w}^t) \\
 &\quad \cdot \mathbf{G}_i^{(t)} \left[\frac{\mathbf{G}^{(t)2}}{(\sqrt{z_t} + \epsilon)(\sqrt{z_{t-1}} + \epsilon)(\sqrt{z_t} + \sqrt{z_{t-1}})} \right] \\
 &= \mathbb{E}_{\xi^{(t)}, \mathcal{S}^{(t)}} \nabla f(\mathbf{w}^t) \\
 &\quad \cdot \mathbf{G}_i^{(t)} \left[\frac{\mathbf{G}^{(t)2}}{(\sqrt{z_t} + \epsilon)(\sqrt{z_{t-1}} + \epsilon)(\sqrt{z_t} + \sqrt{z_{t-1}})} \right] \\
 &\leq \mathbb{E}_{\xi^{(t)}, \mathcal{S}^{(t)}} \nabla f(\mathbf{w}^t) \cdot \mathbf{G}_i^{(t)} \cdot \left[\frac{\mathbf{G}^{(t)2}}{(z_t + \epsilon^2)(\sqrt{z_{t-1}} + \epsilon)} \right].
 \end{aligned}$$

Note that $z_{t-1} \geq \epsilon^2$ holds, as $v_0 \geq \epsilon^2$ by the initialisation specified in Algorithm 2, and the z_t is non-decreasing with respect to t . Consequently, the bound above may be further upper-bounded as follows:

$$\begin{aligned}
 T_2 &\leq \mathbb{E}_{\xi^{(t)}, \mathcal{S}^{(t)}} \eta_c K G^2 \frac{\mathbf{G}^{(t)2}}{(z_t + \epsilon^2)(\sqrt{z_{t-1}} + \epsilon)} \\
 &\quad (\text{since } |\nabla f(\mathbf{w}^t)| \leq G) \\
 &\leq \frac{\eta_c K G^2}{\epsilon} \cdot \mathbb{E}_{\xi^{(t)}, \mathcal{S}^{(t)}} \left[\frac{\mathbf{G}^{(t)2}}{z_t + \epsilon^2} \right] \quad (\text{since } \sqrt{z_{t-1,j}} \geq 0) \\
 &\leq \frac{\eta_c K G^2}{\epsilon^3} \cdot \mathbb{E}_{\xi^{(t)}, \mathcal{S}^{(t)}} [\mathbf{G}^{(t)2}].
 \end{aligned}$$

Now we bound T_1 :

$$\begin{aligned}
 T_1 &= \left\langle \nabla f(\mathbf{w}^t), \mathbb{E} \left[\frac{-\mathbf{G}^{(t)}}{\sqrt{z_{t-1}} + \epsilon} \right] \right\rangle \\
 &= \left\langle \frac{\nabla f(\mathbf{w}^t)}{\sqrt{z_{t-1}} + \epsilon}, \mathbb{E} [-\mathbf{G}^{(t)} - \nabla f(\mathbf{w}^t) + \nabla f(\mathbf{w}^t)] \right\rangle \\
 &= -\frac{1}{\sqrt{z_{t-1}} + \epsilon} \|\nabla f(\mathbf{w}^t)\|^2 + \underbrace{\left\langle \frac{\nabla f(\mathbf{w}^t)}{\sqrt{z_{t-1}} + \epsilon}, \mathbb{E} [-\mathbf{G}^{(t)} + \nabla f(\mathbf{w}^t)] \right\rangle}_{T_3}.
 \end{aligned}$$

Now we bound T_3 :

$$\begin{aligned}
 T_3 &= \left\langle \frac{\nabla f(\mathbf{w}^t)}{\sqrt{z_{t-1}} + \epsilon}, \mathbb{E}[-\mathbf{G}^{(t)} + \nabla f(\mathbf{w}^t)] \right\rangle \\
 &\leq \frac{1}{2} \frac{\|\nabla f(\mathbf{w}^t)\|^2}{\sqrt{z_{t-1}} + \epsilon} + \frac{1}{2\epsilon} \mathbb{E}\|\mathbf{G}^{(t)} - \nabla f(\mathbf{w}^t)\|^2 \\
 &\leq \frac{1}{2\epsilon} \|\nabla f(\mathbf{w}^t)\|^2 + \frac{1}{2\epsilon} \mathbb{E}\|\mathbf{G}^{(t)} - \nabla f(\mathbf{w}^t)\|^2.
 \end{aligned}$$

Then we have:

$$\begin{aligned}
 &\mathbb{E}[f(\mathbf{w}^{t+1})] \\
 &\leq f(\mathbf{w}^t) + \eta_s T_1 + \eta_s T_2 + \frac{\eta_s^2 L}{2\epsilon^2} \mathbf{G}^{(t)} \mathbf{G}^{(t)} \\
 &\leq f(\mathbf{w}^t) - \frac{\eta_s}{\sqrt{z_{t-1}} + \epsilon} \|\nabla f(\mathbf{w}^t)\|^2 + \frac{\eta_s}{2\epsilon} \|\nabla f(\mathbf{w}^t)\|^2 + \frac{\eta_s}{2\epsilon} \mathbb{E}\|\mathbf{G}^{(t)} - \nabla f(\mathbf{w}^t)\|^2 + \left(\frac{\eta_s \eta_c K G^2}{\epsilon^3} + \frac{\eta_s^2 L}{2\epsilon^2}\right) \cdot \mathbb{E}_{\xi^{(t)}, \mathcal{S}^{(t)}} \mathbf{G}^{(t)} \mathbf{G}^{(t)} \\
 &\leq f(\mathbf{w}^t) - \frac{\eta_s}{\sqrt{z_{t-1}} + \epsilon} \|\nabla f(\mathbf{w}^t)\|^2 + \frac{\eta_s}{2\epsilon} \|\nabla f(\mathbf{w}^t)\|^2 + \frac{\eta_s}{2\epsilon} \mathbb{E}\|\mathbf{G}^{(t)} - \bar{h}^{(t)}\|^2 + \frac{\eta_s}{2\epsilon} \|\bar{h}^{(t)} - \nabla f(\mathbf{w}^t)\|^2 \\
 &\quad + \left(\frac{\eta_s \eta_c K G^2}{\epsilon^3} + \frac{\eta_s^2 L}{2\epsilon^2}\right) \cdot \eta_c^2 K^2 M^2 G^2.
 \end{aligned}$$

Based on Lemmas A.6 and A.7, we can define $C^{(t)} \triangleq \frac{1}{N} \sum_{i=1}^N \mathbb{E}_{\xi^{(t)}} \|\nabla f_i(\mathbf{w}^{(t)}) - \mathbf{h}_i^{(t)}\|^2$. Then the following relation holds:

$$\begin{aligned}
 &\mathbb{E}\|\mathbf{G}^{(t)} - \bar{h}^{(t)}\|^2 \\
 &\leq \left(\frac{4}{M} \frac{N-M}{N-1}\right) C^{(t)} + \frac{\sigma^2}{MK} + \left(\frac{4\tilde{\eta}_s^2 L^2}{M} \frac{N-M}{N-1}\right) \|\mathbf{G}^{(t-1)}\|^2 + \left(\frac{2}{M} \frac{N-M}{N-1}\right) \frac{1}{N} \sum_{j=1}^N \|\nabla f_j(\mathbf{w}^{(t-1)}) - \mathbf{y}_j^{(t)}\|^2 \\
 &\leq \left(\frac{4}{M} \frac{N-M}{N-1}\right) C^{(t)} + \frac{\sigma^2}{MK} + \left(\frac{4\tilde{\eta}_s^2 L^2}{M} \frac{N-M}{N-1}\right) \eta_c^2 K^2 M^2 G^2 + \left(\frac{2}{M} \frac{N-M}{N-1}\right) \sigma^2.
 \end{aligned}$$

Then it follows that:

$$\begin{aligned}
 &\mathbb{E}[f(\mathbf{w}^{t+1})] \\
 &\leq f(\mathbf{w}^t) - \frac{\eta_s}{\sqrt{z_{t-1}} + \epsilon} \|\nabla f(\mathbf{w}^t)\|^2 + \frac{\eta_s}{2\epsilon} \|\nabla f(\mathbf{w}^t)\|^2 + \frac{\eta_s}{2\epsilon} \mathbb{E}\|\mathbf{G}^{(t)} - \bar{h}^{(t)}\|^2 + \\
 &\quad \frac{\eta_s}{2\epsilon} C^{(t)} + \left(\frac{\eta_s \eta_c K G^2}{\epsilon^3} + \frac{\eta_s^2 L}{2\epsilon^2}\right) \cdot \eta_c^2 K^2 M^2 G^2 \\
 &\leq f(\mathbf{w}^t) - \frac{\eta_s}{\sqrt{z_{t-1}} + \epsilon} \|\nabla f(\mathbf{w}^t)\|^2 + \frac{\eta_s}{2\epsilon} \|\nabla f(\mathbf{w}^t)\|^2 + \frac{\eta_s}{2\epsilon} \left(1 + \frac{4}{M} \frac{N-M}{N-1}\right) C^{(t)} \\
 &\quad + \frac{\eta_s}{2\epsilon} \left(\frac{\sigma^2}{MK} + \frac{2(N-M)}{M(N-1)}\right) \sigma^2 + \frac{\eta_s}{2\epsilon} \left(\frac{4\tilde{\eta}_s^2 L^2}{M} \frac{N-M}{N-1} + \frac{2\eta_c K G^2}{\epsilon^2} + \frac{\eta_s L}{\epsilon}\right) \eta_c^2 K^2 M^2 G^2 \\
 &\leq f(\mathbf{w}^t) - \frac{\eta_s}{\sqrt{z_{t-1}} + \epsilon} \|\nabla f(\mathbf{w}^t)\|^2 + \frac{\eta_s}{2\epsilon} \|\nabla f(\mathbf{w}^t)\|^2 + \frac{\eta_s}{2\epsilon} \left(1 + \frac{4}{M} \frac{N-M}{N-1}\right) C^{(t)} \\
 &\quad + \frac{\eta_s}{2\epsilon} \left(\frac{1}{MK} + \frac{2(N-M)}{M(N-1)}\right) \sigma^2 + \frac{\eta_s}{2\epsilon} \eta_c^2 K^2 M^2 G^2.
 \end{aligned}$$

Since $C^{(t)} \leq 2\eta_c^2 L^2(K-1)\sigma^2 + 8\eta_c^2 L^2 K(K-1) \left[\sigma_g^2 + \|\nabla f(\mathbf{w}^{(t)})\|^2 \right]$ as established in Lemma 5, it follows that

$$\begin{aligned} \mathbb{E}[f(\mathbf{w}^{t+1})] &\leq f(\mathbf{w}^t) - \frac{\eta_s}{\sqrt{z_{t-1}} + \epsilon} \|\nabla f(\mathbf{w}^t)\|^2 \\ &\quad + \frac{\eta_s}{2\epsilon} \|\nabla f(\mathbf{w}^t)\|^2 + \frac{\eta_s}{2\epsilon} \left(1 + \frac{4(N-M)}{M(N-1)} \right) \left[2\eta_c^2 L^2(K-1)\sigma^2 + 8\eta_c^2 L^2 K(K-1) (\sigma_g^2 + \|\nabla f(\mathbf{w}^t)\|^2) \right] \\ &\quad + \frac{\eta_s}{2\epsilon} \eta_c^2 K^2 M^2 G^2 + \frac{\eta_s}{2\epsilon} \left(\frac{1}{MK} + \frac{2(N-M)}{M(N-1)} \right) \sigma^2. \end{aligned}$$

Define

$$\begin{aligned} B &:= 1 + \frac{4(N-M)}{M(N-1)}, \\ \Gamma &:= \eta_s \left[\frac{1}{\sqrt{z_{t-1}} + \epsilon} - \frac{1}{2\epsilon} (1 + 8B\eta_c^2 L^2 K(K-1)) \right], \\ A_1 &:= 4\eta_c^2 L^2 K(K-1), \\ A_2 &:= \eta_c^2 L^2(K-1) + \frac{\eta_s}{2MK\epsilon} + \frac{\eta_s}{M\epsilon}, \\ A_3 &:= \frac{\eta_s}{2\epsilon^2} \eta_c^2 K^2 M^2 G^2. \end{aligned}$$

Under the condition of η_c and η_S , The inequality then becomes

$$\mathbb{E}[f(\mathbf{w}^{t+1})] \leq f(\mathbf{w}^t) - \Gamma \|\nabla f(\mathbf{w}^t)\|^2 + A_1 \sigma_g^2 + A_2 \sigma^2 + A_3.$$

Rearranging gives

$$\Gamma \|\nabla f(\mathbf{w}^t)\|^2 \leq f(\mathbf{w}^t) - \mathbb{E}[f(\mathbf{w}^{t+1})] + A_1 \sigma_g^2 + A_2 \sigma^2 + A_3.$$

Summing over $t = 0, \dots, T-1$ yields a telescoping sum of the function values:

$$\begin{aligned} \frac{1}{4} \sum_{t=0}^{T-1} \mathbb{E} \|\nabla f(\mathbf{w}^t)\|^2 &\leq \Gamma \sum_{t=0}^{T-1} \mathbb{E} \|\nabla f(\mathbf{w}^t)\|^2 \\ &\leq f(\mathbf{w}^0) - \mathbb{E}[f(\mathbf{w}^T)] + T(A_1 \sigma_g^2 + A_2 \sigma^2 + A_3). \end{aligned}$$

Let f^* denote the minimum value of f . Dividing both sides by $\frac{1}{4}$ then gives:

$$\frac{1}{T} \sum_{t=0}^{T-1} \mathbb{E} \|\nabla f(\mathbf{w}^t)\|^2 \leq \frac{4(f(\mathbf{w}^0) - f^*)}{T} + 4(A_1 \sigma_g^2 + A_2 \sigma^2 + A_3).$$

□

B. Adaptive Optimisers

Any of the five adaptive optimisers may be employed on the server side to compute the global update. The corresponding pseudocode and update rules for these algorithms are presented below.

B.1. Adagrad (Algorithm 3).

Algorithm 3 ADAGRADOPT (Latest model parameters $\mathbf{w}^{(t)}$, pseudo-gradient $\mathbf{G}^{(t)}$, server learning rate η_s , accumulator z_t)

Require: ϵ (small constant), λ (weight decay)

- 1: **if** $\lambda \neq 0$ **then**
- 2: $\mathbf{G}^{(t)} \leftarrow \mathbf{G}^{(t)} + \lambda \mathbf{w}^{(t)}$;
- 3: **end if**
- 4: $z_t \leftarrow z_{t-1} + \mathbf{G}^{(t)} \odot \mathbf{G}^{(t)}$;
- 5: $\mathbf{w}^{(t+1)} \leftarrow \mathbf{w}^{(t)} - \eta_s \frac{\mathbf{G}^{(t)}}{\sqrt{z_t} + \epsilon}$;
- 6: **return** $\mathbf{w}^{(t+1)}$.

The value $\mathbf{G}^{(t)}$, as computed in equation (9), is utilised in the calculation of z_t (accumulator):

$$z_t \leftarrow z_{t-1} + \mathbf{G}^{(t)} \odot \mathbf{G}^{(t)}. \quad (12)$$

Then z_t is used for the global update:

$$\mathbf{w}^{(t+1)} \leftarrow \mathbf{w}^{(t)} - \eta_s \frac{\mathbf{G}^{(t)}}{\sqrt{z_t} + \epsilon}, \quad (13)$$

where ϵ is a small constant.

B.2. Adam (Algorithm 4).

Algorithm 4 ADAMOPT (Latest model parameters $\mathbf{w}^{(t)}$, pseudo-gradient $\mathbf{G}^{(t)}$, server learning rate η_s , moments m_t, v_t)

Require: Decay rates β_1, β_2 , small constant ϵ , weight decay λ

- 1: **if** $\lambda \neq 0$ **then**
- 2: $\mathbf{G}^{(t)} \leftarrow \mathbf{G}^{(t)} + \lambda \mathbf{w}^{(t)}$;
- 3: **end if**
- 4: $m_t \leftarrow \beta_1 m_{t-1} + (1 - \beta_1) \mathbf{G}^{(t)}$;
- 5: $v_t \leftarrow \beta_2 v_{t-1} + (1 - \beta_2) (\mathbf{G}^{(t)} \odot \mathbf{G}^{(t)})$;
- 6: $\hat{m}_t \leftarrow \frac{m_t}{1 - \beta_1^T}$;
- 7: $\hat{v}_t \leftarrow \frac{v_t}{1 - \beta_2^T}$;
- 8: $\mathbf{w}^{(t+1)} \leftarrow \mathbf{w}^{(t)} - \eta_s \frac{\hat{m}_t}{\sqrt{\hat{v}_t} + \epsilon}$;
- 9: **return** $\mathbf{w}^{(t+1)}$.

The $\mathbf{G}^{(t)}$, obtained from the equation (9), is employed to compute the moments m_t and v_t , both of which are initially set to 0. The hyperparameters β_1 and β_2 are also required for the computation of m_t and v_t :

$$m_t \leftarrow \beta_1 m_{t-1} + (1 - \beta_1) \mathbf{G}^{(t)}; \quad (14)$$

$$v_t \leftarrow \beta_2 v_{t-1} + (1 - \beta_2) (\mathbf{G}^{(t)} \odot \mathbf{G}^{(t)}). \quad (15)$$

The moments m_t and v_t are subsequently utilised to compute \hat{m}_t and \hat{v}_t :

$$\hat{m}_t \leftarrow \frac{m_t}{1 - \beta_1^T}; \quad (16)$$

$$\hat{v}_t \leftarrow \frac{v_t}{1 - \beta_2^T}. \quad (17)$$

Here, \mathcal{T} denotes the iteration counter (server round in the proposed algorithms). The values \hat{m}_t and \hat{v}_t are then employed to compute the global update:

$$\mathbf{w}^{(t+1)} \leftarrow \mathbf{w}^{(t)} - \eta_s \frac{\hat{m}_t}{\sqrt{\hat{v}_t} + \epsilon}, \quad (18)$$

where ϵ is a small constant.

B.3. Adabelief (Algorithm 5).

Algorithm 5 ADABELIEFOPT (Latest model parameters $\mathbf{w}^{(t)}$, pseudo-gradient $\mathbf{G}^{(t)}$, server learning rate η_s , moments m_t, z_t)

Require: Decay rates β_1, β_2 , small constant ϵ , weight decay λ

- 1: **if** $\lambda \neq 0$ **then**
- 2: $\mathbf{G}^{(t)} \leftarrow \mathbf{G}^{(t)} + \lambda \mathbf{w}^{(t)}$;
- 3: **end if**
- 4: $m_t \leftarrow \beta_1 m_{t-1} + (1 - \beta_1) \mathbf{G}^{(t)}$;
- 5: $z_t \leftarrow \beta_2 z_{t-1} + (1 - \beta_2) (\mathbf{G}^{(t)} - m_t)^2$;
- 6: $\hat{m}_t \leftarrow \frac{m_t}{1 - \beta_1^T}$;
- 7: $\hat{z}_t \leftarrow \frac{z_t}{1 - \beta_2^T}$;
- 8: $\mathbf{w}^{(t+1)} \leftarrow \mathbf{w}^{(t)} - \eta_s \frac{\hat{m}_t}{\sqrt{\hat{z}_t} + \epsilon}$;
- 9: **return** $\mathbf{w}^{(t+1)}$.

The $\mathbf{G}^{(t)}$, obtained in the equation (9), is used to compute the moments m_t and z_t , both of which are initially set to 0. The hyperparameters β_1 and β_2 are also required for the computation of m_t and z_t .

$$m_t \leftarrow \beta_1 m_{t-1} + (1 - \beta_1) \mathbf{G}^{(t)}; \quad (19)$$

$$z_t \leftarrow \beta_2 z_{t-1} + (1 - \beta_2) (\mathbf{G}^{(t)} - m_t)^2. \quad (20)$$

The moments m_t and z_t are subsequently used to compute \hat{m}_t and \hat{z}_t :

$$\hat{m}_t \leftarrow \frac{m_t}{1 - \beta_1^T}; \quad (21)$$

$$\hat{z}_t \leftarrow \frac{z_t}{1 - \beta_2^T}. \quad (22)$$

Here, \mathcal{T} denotes the iteration counter (server round in the proposed algorithms). The values \hat{m}_t and \hat{z}_t are then employed to compute the global update:

$$\mathbf{w}^{(t+1)} \leftarrow \mathbf{w}^{(t)} - \eta_s \frac{\hat{m}_t}{\sqrt{\hat{z}_t} + \epsilon}, \quad (23)$$

where ϵ is a small constant.

B.4. Yogi (Algorithm 6).

Algorithm 6 YOGIOPT (Latest model parameters $\mathbf{w}^{(t)}$, pseudo-gradient $\mathbf{G}^{(t)}$, server learning rate η_s , moments m_t, v_t)

Require: Decay rates β_1, β_2 , small constant ϵ , and weight decay λ

- 1: **if** $\lambda \neq 0$ **then**
- 2: $\mathbf{G}^{(t)} \leftarrow \mathbf{G}^{(t)} + \lambda \mathbf{w}^{(t)}$;
- 3: **end if**
- 4: $m_t \leftarrow \beta_1 m_{t-1} + (1 - \beta_1) \mathbf{G}^{(t)}$;
- 5: $v_t \leftarrow v_{t-1} - (1 - \beta_2) \mathbf{G}^{(t)} \odot \mathbf{G}^{(t)} \operatorname{sgn}(v_{t-1} - \mathbf{G}^{(t)} \odot \mathbf{G}^{(t)})$;
- 6: $\hat{m}_t \leftarrow \frac{m_t}{1 - \beta_1^T}$;
- 7: $\hat{v}_t \leftarrow \frac{v_t}{1 - \beta_2^T}$;
- 8: $\mathbf{w}^{(t+1)} \leftarrow \mathbf{w}^{(t)} - \eta_s \frac{\hat{m}_t}{\sqrt{\hat{v}_t} + \epsilon}$;
- 9: **return** $\mathbf{w}^{(t+1)}$.

The $\mathbf{G}^{(t)}$ calculated in the equation (9) is used to compute the moments m_t and v_t , which are initially set to 0. The hyperparameters β_1 and β_2 are also required for calculating m_t and v_t :

$$m_t \leftarrow \beta_1 m_{t-1} + (1 - \beta_1) \mathbf{G}^{(t)}; \quad (24)$$

$$v_t \leftarrow v_{t-1} - (1 - \beta_2) \mathbf{G}^{(t)} \odot \mathbf{G}^{(t)} \operatorname{sgn}(v_{t-1} - \mathbf{G}^{(t)} \odot \mathbf{G}^{(t)}). \quad (25)$$

The m_t and v_t are then used to compute \hat{m}_t and \hat{v}_t :

$$\hat{m}_t \leftarrow \frac{m_t}{1 - \beta_1^T}; \quad (26)$$

$$\hat{v}_t \leftarrow \frac{v_t}{1 - \beta_2^T}. \quad (27)$$

Here, \mathcal{T} denotes the iteration counter (server round in the algorithms). Subsequently, \hat{m}_t and \hat{v}_t are utilised for the global update:

$$\mathbf{w}^{(t+1)} \leftarrow \mathbf{w}^{(t)} - \eta_s \frac{\hat{m}_t}{\sqrt{\hat{v}_t} + \epsilon}, \quad (28)$$

where ϵ is a small constant.

B.5. Lamb (Algorithm 7).

Algorithm 7 LAMBOPT (Latest model parameters $\mathbf{w}^{(t)}$, pseudo-gradient $\mathbf{G}^{(t)}$, server learning rate η_s , moments m_t, v_t)

Require: Decay rates β_1, β_2 , small constant ϵ , and weight decay λ

```

1: if  $\lambda \neq 0$  then
2:    $\mathbf{G}^{(t)} \leftarrow \mathbf{G}^{(t)} + \lambda \mathbf{w}^{(t)};$ 
3: end if
4:  $m_t \leftarrow \beta_1 m_{t-1} + (1 - \beta_1) \mathbf{G}^{(t)};$ 
5:  $v_t \leftarrow \beta_2 v_{t-1} + (1 - \beta_2) (\mathbf{G}^{(t)} \odot \mathbf{G}^{(t)});$ 
6:  $\hat{m}_t \leftarrow \frac{m_t}{1 - \beta_1^T};$ 
7:  $\hat{v}_t \leftarrow \frac{v_t}{1 - \beta_2^T};$ 
8:  $\hat{r}_t \leftarrow \frac{\hat{m}_t}{\sqrt{\hat{v}_t} + \epsilon};$ 
9:  $weight\_norm \leftarrow \|\mathbf{w}^{(t)}\|;$ 
10:  $update\_norm \leftarrow \|\hat{r}_t\|;$ 
11: if  $weight\_norm > 0$  and  $update\_norm > 0$  then
12:    $r_t \leftarrow \frac{weight\_norm}{update\_norm};$ 
13: else
14:    $r_t \leftarrow 1.0;$ 
15: end if
16:  $\mathbf{w}^{(t+1)} \leftarrow \mathbf{w}^{(t)} - \eta_s r_t \hat{r}_t;$ 
17: return  $\mathbf{w}^{(t+1)}.$ 

```

$\mathbf{G}^{(t)}$ calculated in the equation (9) is used to compute the moments m_t and v_t , both initially set to 0. The hyperparameters β_1 and β_2 are also required to calculate m_t and v_t :

$$m_t \leftarrow \beta_1 m_{t-1} + (1 - \beta_1) \mathbf{G}^{(t)}; \quad (29)$$

$$v_t \leftarrow \beta_2 v_{t-1} + (1 - \beta_2) (\mathbf{G}^{(t)} \odot \mathbf{G}^{(t)}). \quad (30)$$

The m_t and v_t are then used to compute \hat{m}_t and \hat{v}_t :

$$\hat{m}_t \leftarrow \frac{m_t}{1 - \beta_1^T}; \quad (31)$$

$$\hat{r}_t \leftarrow \frac{\hat{m}_t}{\sqrt{\hat{v}_t} + \epsilon}; \quad (32)$$

$$\hat{v}_t \leftarrow \frac{v_t}{1 - \beta_2^T}; \quad (33)$$

Here, \mathcal{T} denotes the iteration counter (server round in the algorithms). Then, $\mathbf{w}^{(t)}$ and \hat{r}_t are used to calculate:

$$weight_norm \leftarrow \|\mathbf{w}^{(t)}\|; \quad (34)$$

$$update_norm \leftarrow \|\hat{r}_t\|; \quad (35)$$

$$r_t = \begin{cases} \frac{weight_norm}{update_norm} & weight_norm \neq 0 \text{ and } update_norm \neq 0 \\ r_t \leftarrow 1.0 & \end{cases}. \quad (36)$$

Then, r_t and \hat{r}_t are used for the global update:

$$\mathbf{w}^{(t+1)} \leftarrow \mathbf{w}^{(t)} - \eta_s r_t \hat{r}_t. \quad (37)$$

C. Model Quantisation

While various quantisation paradigms exist, we focus on three distinct strategies for compressing stored client updates. Algorithm 8 details the use of FP16 (half-precision), Int8, and Int4 quantisation, complemented by the corresponding dequantisation procedures in Algorithm 9. These methods achieve server-side memory reductions of 50%, 75%, and 87.5%, respectively. We provide experimental validation of these integer-based formats; however, a comprehensive evaluation of alternative quantisation schemes is beyond the scope of this work due to computational constraints. For 8-bit quantisation we use the symmetric per-tensor uniform quantiser of (Krishnamoorthi, 2018), and for 4-bit quantisation we follow (Zhou et al., 2016), packing two 4-bit values per byte for storage. Values are scaled by the tensor maximum; per-channel/asymmetric alternatives exist but are out of scope.

Algorithm 8 QUANT($\mathbf{g}_j^{(t)}$)

```

1: Initialisation: Set mode                                ▷ Initialise quantisation mode (eg: FP16, Int8, Int4).
2:  $\mathcal{Q} \leftarrow \emptyset$ ;                                     ▷ Initialise list to store compressed layers
3: for all  $\mathbf{W}$  in  $\mathbf{g}_j^{(t)}$  do
4:   if mode = FP16 then
5:      $\mathbf{W}_q \leftarrow \text{cast}(\mathbf{W}, \text{float16});$ 
6:     Append  $\mathbf{W}_q$  to  $\mathcal{Q}$ ;
7:   else if mode = Int8 then
8:      $\alpha \leftarrow \max(|\mathbf{W}|)/127;$                                 ▷ Scale for signed 8-bit
9:      $\alpha \leftarrow 1.0$  if  $\alpha = 0;$ 
10:     $\mathbf{W}_{\text{int}} \leftarrow \text{cast}(\text{clip}(\text{round}(\mathbf{W}/\alpha), -127, 127), \text{int8});$ 
11:    Append  $(\mathbf{W}_{\text{int}}, \alpha)$  to  $\mathcal{Q}$ ;                                ▷ Store Int8 tensor and scale
12:   else if mode = Int4 then
13:      $S \leftarrow \text{shape}(\mathbf{W});$ 
14:      $\alpha \leftarrow \max(|\mathbf{W}|)/7;$                                 ▷ Scale for signed 4-bit
15:      $\alpha \leftarrow 1.0$  if  $\alpha = 0;$ 
16:      $\mathbf{W}_{\text{int}} \leftarrow \text{clip}(\text{round}(\mathbf{W}/\alpha), -7, 7);$ 
17:      $\mathbf{W}_{\text{flat}} \leftarrow \text{flatten}(\mathbf{W}_{\text{int}} + 8);$                                 ▷ Shift to [1, 15] and flatten
18:      $\mathbf{P} \leftarrow \emptyset;$ 
19:     for  $k = 0, 2, \dots, \text{length}(\mathbf{W}_{\text{flat}}) - 1$  do
20:        $h \leftarrow \mathbf{W}_{\text{flat}}[k] \ll 4;$                                 ▷ High 4 bits
21:        $l \leftarrow \mathbf{W}_{\text{flat}}[k + 1];$                                 ▷ Low 4 bits
22:       Append  $(h \vee l)$  to  $\mathbf{P};$                                 ▷ Pack into Uint8
23:     end for
24:     Append  $(\mathbf{P}, \alpha, S)$  to  $\mathcal{Q}$ ;                                ▷ Store packed data, scale, and shape
25:   end if
26: end for
27: return  $\mathcal{Q}.$ 

```

D. Experimental Setup

D.1. Datasets

To conduct the experiments, we utilised three publicly available vision classification datasets and one next-character prediction text dataset. Brief descriptions of these datasets are provided below.

Algorithm 9 DEQUANT(\mathcal{Q})

```

1: Initialisation: Set mode                                 $\triangleright$  Initialise dequantisation mode (eg: FP16, Int8, Int4).
2:  $\mathcal{W}_{\text{restored}} \leftarrow \emptyset$ ;
3: for all item in  $\mathcal{Q}$  do
4:   if mode = FP16 then
5:      $\mathbf{W}_{\text{float}} \leftarrow \text{cast}(\text{item}, \text{float32})$ ;
6:     Append  $\mathbf{W}_{\text{float}}$  to  $\mathcal{W}_{\text{restored}}$ ;
7:   else if mode = Int8 then
8:      $(\mathbf{W}_{\text{int}}, \alpha) \leftarrow \text{item}$ ;
9:      $\mathbf{W}_{\text{float}} \leftarrow \text{cast}(\mathbf{W}_{\text{int}}, \text{float32}) \times \alpha$ ;            $\triangleright$  Restore scale
10:    Append  $\mathbf{W}_{\text{float}}$  to  $\mathcal{W}_{\text{restored}}$ ;
11:   else if mode = Int4 then
12:      $(\mathbf{P}, \alpha, S) \leftarrow \text{item}$ ;            $\triangleright$  Unpack tuple: Packed data, scale, shape
13:      $N \leftarrow \prod_{d \in S} d$ ;            $\triangleright$  Total elements
14:      $\mathbf{U}_{\text{even}} \leftarrow (\mathbf{P} \gg 4)$ ;            $\triangleright$  Extract high 4 bits
15:      $\mathbf{U}_{\text{odd}} \leftarrow (\mathbf{P} \& 0x0F)$ ;            $\triangleright$  Extract low 4 bits
16:      $\mathbf{U} \leftarrow \text{Interleave}(\mathbf{U}_{\text{even}}, \mathbf{U}_{\text{odd}})$ ;            $\triangleright$  Vectorised merge
17:      $\mathbf{U} \leftarrow \mathbf{U}[0 : N]$ ;            $\triangleright$  Remove padding if any
18:      $\mathbf{W}_{\text{signed}} \leftarrow \text{cast}(\mathbf{U}, \text{int8}) - 8$ ;            $\triangleright$  Reverse shift offset
19:      $\mathbf{W}_{\text{float}} \leftarrow \text{reshape}(\text{cast}(\mathbf{W}_{\text{signed}}, \text{float32}) \times \alpha, S)$ ;
20:     Append  $\mathbf{W}_{\text{float}}$  to  $\mathcal{W}_{\text{restored}}$ ;
21:   end if
22: end for
23: return  $\mathcal{W}_{\text{restored}}$ .

```

- **MNIST (Deng, 2012).** The MNIST dataset contains 60,000 handwritten digit images (50,000 for training and 10,000 for testing) across 10 classes. Each image is a 28x28 grayscale image.
- **FMNIST (Xiao et al., 2017).** The FMNIST dataset consists of 60,000 training and 10,000 test images of fashion items, each as a 28x28 grayscale image across 10 classes.
- **CIFAR-10 (Krizhevsky, 2009).** The CIFAR-10 dataset comprises 60,000 colour images (50,000 for training and 10,000 for testing) of size 32x32 across 10 classes.
- **Shakespeare (Caldas et al., 2018).** This dataset built from The Complete Works of William Shakespeare. We used Flower (Beutel et al., 2020) Hugging Face repository to download this dataset where total number of samples are 4,226,158. Here, each speaking role in each play is considered a different device which is 1129.

D.2. Dataset Partitioning Method

In our experiments, data were partitioned into an Independent and Identically Distributed (IID) setting and five distinct Non-Independent and Identically Distributed (non-IID) settings. Specifically, the vision datasets were partitioned based on label skewness, whereas the Shakespeare dataset utilised a Natural ID partitioning strategy. These settings include:

- **IID:** Data are uniformly distributed across labels with no skewness. In this FL IID setting, each client receives an equal amount of data from every class.
- **IID-Non_IID:** A hybrid setting in which 50% of the data follows an IID distribution, while the remainder follows a non-IID distribution. The notation Non_IID is used instead of IID-Non_IID for clarity in the tables.
- **Dirichlet:** A non-IID scenario where data points are assigned to clients according to a Dirichlet distribution. The parameter β governs the degree of skewness; smaller β values indicate greater skew, whereas larger β values approximate an IID distribution. In the experiments, $\beta = 0.5$ was employed.
- **Sort and Partition:** Here, data are initially sorted by label and then partitioned into C chunks. A value of $C = 1$ implies that each partition contains data from only one class, representing the most extreme non-IID setting. Values $C = 1, 2, 3$ denote increasing breadth of data distribution. In this study, LQ-1, LQ-2, and LQ-3 refer to data sorted by label and partitioned into 1, 2, and 3 chunks, respectively.

- **Natural ID Partitioner:** Unlike synthetic splitting strategies, this method preserves the inherent user-based segmentation present in the raw data. By allocating data according to the identifiers, this setting captures the realistic, non-IID statistical heterogeneity and feature distribution.

Further details regarding these partitioning methods are provided in (Li et al., 2022b) and the official Flower documentation (Beutel et al., 2020).

D.3. Experimental and Hyperparameters setup

Table 1. Experimental and hyperparameter setup.

PARAMETER	DATASET			
	MNIST	F-MNIST	CIFAR-10	SHAKESPEARE
# OF CLIENTS	500	500	250	904
# OF PARTICIPATING CLIENTS	5	5	5	5
% OF PARTICIPATING CLIENTS	1%	1%	2%	< 1%
# OF CLIENTS FOR EVALUATION	250	250	250	225
LOCAL MODEL	LENET-5	LENET-5	RESNET-18	GRU
BATCH SIZE	20	20	20	64
LOCAL EPOCHS	1	3	5	5
CLIENT LEARNING RATE η_c	0.1, 0.01, 0.001			
CLIENT MOMENTUM	0.9			
DECAY RATE β_1	0.9			
DECAY RATE β_2	0.999			
SMALL CONSTANT ϵ	$1e^{-8}$			
WEIGHT DECAY λ	0			

The experimental setup utilises a range of parameters and hyperparameters. Table 1 offers a detailed summary of the configurations, parameters, and hyperparameters employed. The algorithms MIFA, FedVARP, FEDADAVR, and FEDADAVR-QUANT were implemented using the Flower framework alongside PyTorch. For other baseline algorithms already available within Flower, such as FedAvg, FedAdagrad, FedAdam, and FedYogi, default hyperparameter values provided by Flower (i.e. decay rates, small constants, and weight decay) were utilised. Implementation drew upon the repositories from the official Flower (Beutel et al., 2020) federated learning GitHub repository. The same repositories supported the implementation of FedProx, SCAFFOLD, and FedNova. All experiments were executed on high-performance computing systems equipped with CPUs and GPUs.

Table 2. Number of rounds and number of selected rounds average based on data partition.

TYPE	DATASET	PARTITION						NATURAL ID PARTITIONER
		IID	NON_IID	DIRICHLET	LQ-1	LQ-2	LQ-3	
TRAINING ROUNDS	MNIST	60	60	60	100	60	60	X
	F-MNIST	100	100	150	350	150	150	X
	CIFAR-10	200	300	400	1500	500	500	X
	SHAKESPEARE	X	X	X	X	X	X	200
SELECTED ROUNDS	MNIST	10	10	10	10	10	10	X
	F-MNIST	10	10	15	35	25	15	X
	CIFAR-10	20	30	40	150	50	50	X
	SHAKESPEARE	X	X	X	X	X	X	20

Convergence speed varies according to the dataset and the complexity of the data partitioning method. Consequently, the number of federated learning rounds was adjusted per setting, with more rounds for complex scenarios and fewer for simpler ones. Due to notable performance fluctuations between rounds, average accuracy is reported over the final rounds (typically the last 10% of total rounds) in Tables 6, 7, 8, and 9. Table 2 summarises the total rounds and the subset of final rounds used for averaging, according to the data partition. For instance, in the LQ-1 partitioning of the CIFAR-10 dataset, 1500 FL rounds were conducted, with results from the last 150 rounds averaged.

E. Impact of Variance Reduction and Adaptive Optimisation

To rigorously evaluate the individual contributions of our proposed components, we conduct an ablation study comparing the full FEDADAVR algorithm against two dismantled variants: (i) FEDADAVR-NoVR, which removes the variance reduction mechanism while retaining the optimiser (Adagrad for this case); and (ii) FEDADAVR-NoOPT, which removes the server-side adaptive optimiser while retaining variance reduction. All ablation experiments are performed on the CIFAR-10 dataset under the LQ-1 partitioning scheme, strictly adhering to the experimental protocols and hyperparameter settings detailed in Table 1 (with $\eta_s = \eta_c = 0.01$).

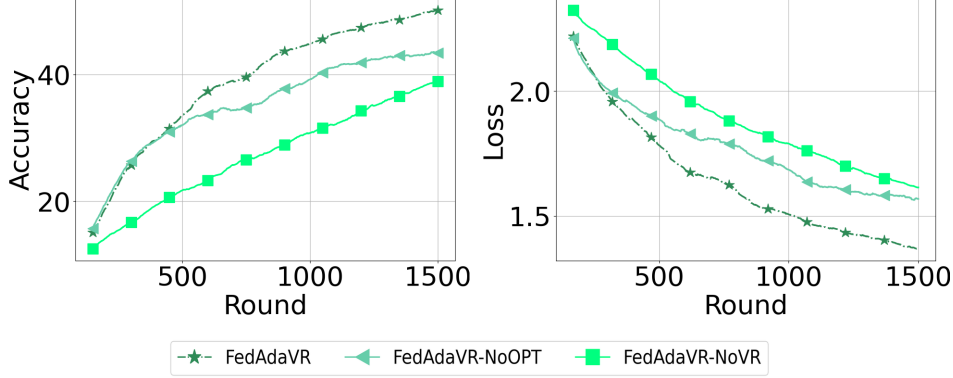


Figure 2. Ablation study analysing the impact of variance reduction and the adaptive optimiser. The plots compare accuracy (left) and loss (right) across FEDADAVR, FEDADAVR-NOOPT, and FEDADAVR-NoVR on the CIFAR-10 dataset (LQ-1 partitioning).

Figure 2 illustrates the convergence trajectories of these variants. As expected, FEDADAVR demonstrates clear superiority, achieving the lowest loss and highest accuracy, even though it initially performed the same as FEDADAVR-NoVR. Specifically, we observe that removing variance reduction (FEDADAVR-NoVR) results in high variance and, consequently, lower accuracy in later rounds, confirming that the SAGA-style VR technique is crucial for mitigating variance arising from partial client participation. Conversely, removing the adaptive optimiser (FEDADAVR-NoOPT) results in slower convergence, highlighting the necessity of the adaptive optimiser for efficient training. These results confirm that the performance gains of FEDADAVR come from the synergistic combination of variance reduction and adaptive optimisation, rather than either component in isolation.

F. Experimental Results

F.1. Accuracy Comparison with State-of-the-Art Methods

F.1.1. ACCURACY AND LOSS COMPARISON WITH THE IID DATA PARTITIONING METHOD (VISION DATASETS).

Figures 1 and 3 illustrate the accuracy and loss of various state-of-the-art methods alongside the two variants of FEDADAVR. In every instance, FEDADAVR surpasses the existing state-of-the-art algorithms. Although FedYogi performs comparatively well, it remains inferior to FEDADAVR under this straightforward data partitioning.

F.1.2. ACCURACY AND LOSS COMPARISON WITH THE IID-NON_IID DATA PARTITIONING METHOD (VISION DATASETS).

From Figures 1 and 3, the accuracy and loss of various state-of-the-art methods alongside the two variants of FEDADAVR under the IID-Non_IID data partitioning method are presented. FEDADAVR and FEDADAVR-QUANT consistently outperforms existing state-of-the-art approaches.

F.1.3. ACCURACY AND LOSS COMPARISON WITH THE DIRICHLET DATA PARTITIONING METHOD (VISION DATASETS).

Figures 1 and 3 demonstrate that the two variants of FEDADAVR outperform existing state-of-the-art methods. While FedYogi performs close to FEDADAVR and FEDADAVR-QUANT on the MNIST and FMNIST datasets, it falls behind on the CIFAR-10 dataset.

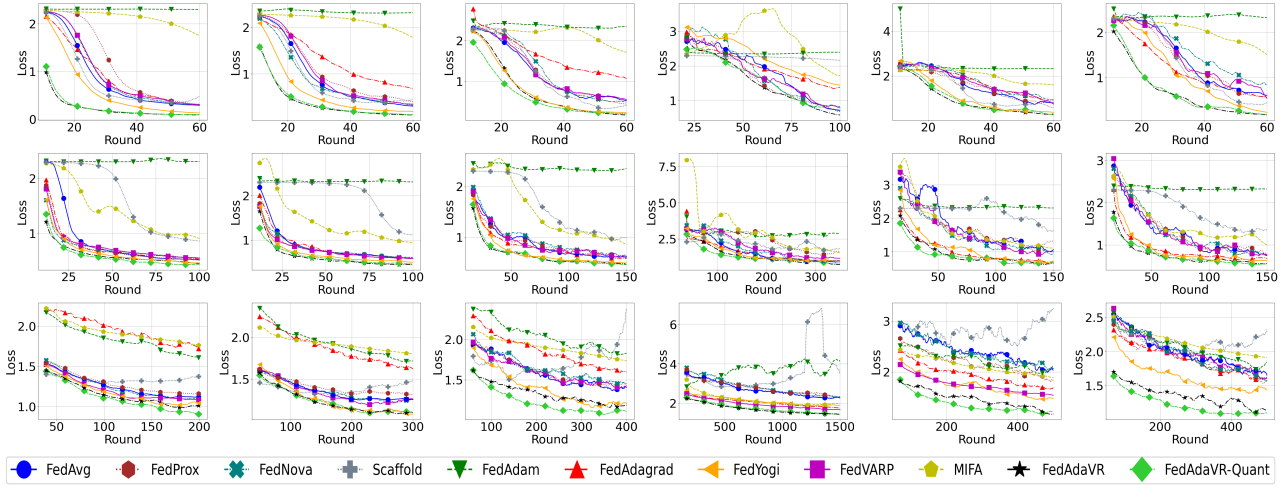


Figure 3. Loss Comparison Across Different Data Partitioning Methods—IID, IID-NonIID, Dirichlet, LQ-1, LQ-2, and LQ-3 (From Left to Right)—on MNIST (Top), FMNIST (Middle), and CIFAR-10 (Bottom) Datasets.

F.1.4. ACCURACY AND LOSS COMPARISON WITH LQ-1 DATA PARTITIONING METHOD (VISION DATASETS).

Figures 1 and 3 illustrate that the two variants of FEDADAVR significantly outperform existing state-of-the-art methods on the CIFAR-10 dataset, which represents the most challenging scenario. Although FedVARP performs well, it remains notably behind both FEDADAVR-QUANT and FEDADAVR. This clearly demonstrates the superiority of the adaptivity to variance reduction approach in extreme cases. Furthermore, FEDADAVR and FEDADAVR-QUANT exhibit faster convergence than other state-of-the-art methods on the MNIST and FMNIST datasets.

F.1.5. ACCURACY AND LOSS COMPARISON WITH LQ-2 DATA PARTITIONING METHOD (VISION DATASETS).

Figures 1 and 3 demonstrate that the two variants of FEDADAVR outperform existing state-of-the-art methods. While FedYogi performs comparably to FEDADAVR and FEDADAVR-QUANT on the MNIST dataset, all state-of-the-art models lag significantly behind on the CIFAR-10 dataset.

F.1.6. ACCURACY AND LOSS COMPARISON WITH LQ-3 DATA PARTITIONING METHOD (VISION DATASETS).

Figures 1 and 3 show that FEDADAVR and FEDADAVR-QUANT consistently outperform existing state-of-the-art methods. Although FedAdagrad and FedYogi performs comparably on the FMNIST dataset, a clear performance gap is evident in other experiments.

F.1.7. ACCURACY AND LOSS COMPARISON ON SHAKESPEARE DATASET (NATURAL ID PARTITIONER).

As illustrated in Figure 4, both FEDADAVR and its quantised variant, FEDADAVR-QUANT, outperform existing state-of-the-art methods on the Shakespeare dataset, with the exception of FedAdagrad. While the margin is narrower here compared to vision experiments, FEDADAVR remains robust; it matches FedAdagrad on this specific task while strictly outperforming it across all other benchmarks.

In summary, FEDADAVR and FEDADAVR-QUANT consistently outperform existing state-of-the-art methods. While FedYogi demonstrates comparable performance on the MNIST and FMNIST datasets, and FedAdagrad achieves similar results on the Shakespeare dataset, a pronounced performance gap emerges under the LQ data partitioning scheme on the more complex CIFAR-10 dataset. Given the greater complexity of CIFAR-10 relative to MNIST, FMNIST, and Shakespeare, convergence rates are slower across all algorithms. Real-world datasets are typically even more complex, featuring highly heterogeneous data distributions among clients. Therefore, federated learning algorithms must be designed to address such challenges effectively. Crucially, FEDADAVR does not discard client updates due to staleness; instead, it adheres to a SAGA-like structure that assumes virtual full participation by retaining all historical updates. While implementing a mechanism to prune excessively stale updates could theoretically enhance efficiency, this investigation remains outside the scope of our current research. Both proposed algorithms, FEDADAVR and FEDADAVR-QUANT, are deemed well-suited to real-world federated learning scenarios.

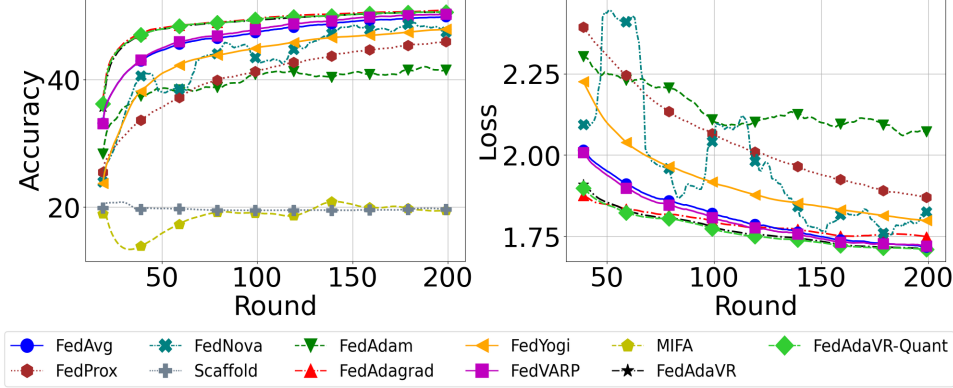


Figure 4. Accuracy and loss comparison on Shakespeare dataset (Natural ID Partitioner). Note that Scaffold and MIFA are omitted from the loss plots due to excessive out-of-range fluctuations.

F.2. Comparison of Experimental Results Between FEDADAVER and FedAdaVR-Quant Using Various Adaptive Optimisers

Tables 6, 7, 8, and 9 present a comparative analysis of experimental results for FEDADAVER and FEDADAVER-QUANT across various adaptive optimisers and datasets. FedVAPR is also included, as it utilises a server learning rate η_s . Bold text denotes the optimiser achieving the highest performance. Lamb consistently attains the best results on the CIFAR-10 dataset, whereas no definitive frontrunner emerges for the other datasets. Consequently, Lamb appears to be the preferred optimiser for more complex datasets such as CIFAR-10. While Adagrad emerges as the top-performing optimiser on the Shakespeare dataset, it demonstrates robust but sub-optimal performance across the vision datasets, where it consistently achieves competitive results without securing the highest accuracy in any evaluated setting.

F.2.1. COMPARISON BETWEEN DIFFERENT QUANTISATION METHOD

In our experiments, client-server communication retained the original FP32 format. However, for server-side storage of client weights, we evaluated varying precision levels: FP32 (full precision), FP16 (half-precision), Int8, and Int4. While storing client states typically requires $\mathcal{O}(Nd)$ memory, employing FP16, Int8, or Int4 quantisation reduces this footprint by 50%, 75%, and 87.5%, respectively. Our results indicate that applying these quantisation methods to the stored updates has a negligible impact on convergence. We attribute this robustness to the fact that quantisation errors are randomly distributed, leading to an inconsequential deviation that does not materially affect the performance of the FL algorithm. Consequently, the quantised versions of FEDADAVER achieve performance comparable to the full-precision baseline, as illustrated in Figure 5. We validated these findings on the CIFAR-10 dataset (LQ-1 distribution) with server learning rate η_s and client learning rate η_c both fixed at 0.001. Given that cross-device settings may involve thousands of resource-constrained clients, the $\mathcal{O}(Nd)$ storage complexity is a critical consideration. Table 3 details the estimated memory requirements for each precision variant across representative model architectures, demonstrating the deployment feasibility of FEDADAVER in cross-device settings.

F.2.2. SERVER LEARNING RATE AND OPTIMISER SELECTION

Experimental findings indicate that for a given optimiser, the performance difference is marginal. On the MNIST and FMNIST datasets, the LeNet-5 model achieves superior results with a higher server learning rate in most scenarios. Conversely, for ResNet-18 on CIFAR-10, a lower server learning rate facilitates faster convergence. These observations underscore the critical sensitivity of algorithm performance to the server learning rate.

Experimental results also indicate on more complex datasets, such as CIFAR-10 under the LQ-1 partition, a lower server learning rate is more effective than a higher one. All optimisers integrated into the algorithms show competitive performance across tasks. For instance, although the Lamb optimiser achieves the highest accuracy in the most complex CIFAR-10 dataset, it converges slowly on the MNIST and FMNIST datasets. Given the black-box characteristics of federated learning, selecting an optimal optimiser remains non-trivial. Nevertheless, all optimisers employed in the proposed algorithms consistently outperform existing baselines. Although five commonly used optimisers were evaluated in this work, other

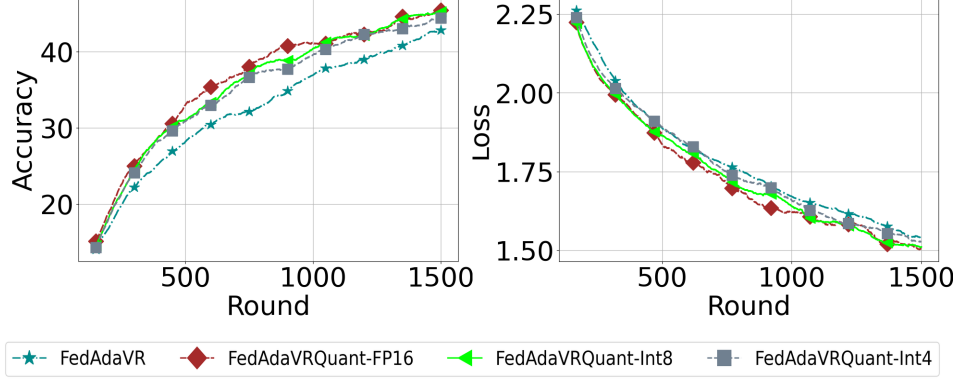


Figure 5. Ablation study on the impact of variance reduction and optimiser. The plots compare accuracy and loss across FEDADAVR, FEDADAVR-NoOPT, and FEDADAVR-NOVR on CIFAR-10 dataset (LQ-1 partitioning).

contemporary or related variants could be readily incorporated.

F.3. FEDADAVR’s Communication Comparison with State-of-the-Art Methods

In our experiments, we selected nine state-of-the-art federated algorithms for comparative evaluation. Among these, only SCAFFOLD incurs the additional communication overhead of transmitting dual parameters (model weights and control variates) during both uplink and downlink. In contrast, FEDADAVR and FEDADAVR-QUANT maintain the standard communication footprint of transmitting only model weights. Due to their superior convergence rates, our proposed methods require significantly fewer total communication rounds compared to the baselines. Table 4 details the number of federated rounds required by each algorithm to achieve specific target accuracy thresholds on the CIFAR-10 dataset under the LQ-1 partitioning strategy. Additionally, we report the normalised communication cost (“Norm. Rounds”) relative to FEDADAVR. The results demonstrate that both FEDADAVR and FEDADAVR-QUANT require significantly fewer rounds than the majority of baselines, thereby substantially reducing the overall communication overhead.

F.4. FEDADAVR’s Computational Latency Comparison with State-of-the-Art Methods

Computational latency in federated learning is governed by diverse factors, including hardware constraints, algorithmic design, and client participation density. To ensure a standardised comparison, we report the average wall-clock time per communication round. All experiments were conducted on a workstation equipped with a 13th Gen Intel Core i9-13900H CPU (2.60 GHz), 64 GB of RAM, and an NVIDIA GeForce RTX 4080 Laptop GPU (12 GB VRAM).

FEDADAVR is designed to impose no additional computational burden on clients; consequently, the client-side execution path is identical to that of FedAvg. However, the server incurs additional computational overhead to mitigate variance. Specifically, the calculation of the correction term $r^{(t)}$ necessitates the aggregation of historical updates from all clients. As our algorithm explicitly accommodates dynamic client participation by allowing clients to join or depart arbitrarily, managing these historical states inevitably increases computation time. As evidenced in Table 5, FEDADAVR exhibits higher latency than most baselines, with the exception of SCAFFOLD. This increase is a direct consequence of the design choices required to handle dynamic environments. While this process could be further optimised for scenarios with fixed client sets, such implementation details are beyond the scope of this work.

Table 3. Estimated server-side memory requirements for storing client states in FEDADAVR. We report the total storage (in Gigabytes) required for varying population sizes (N , in thousands) across popular architectures.

LOCAL MODEL	PARAMETERS (MILLIONS)	# OF CLIENTS (THOUSANDS)	APPROXIMATE MEMORY (GIGABYTES)			
			FP32	FP16	INT8	INT4
SQUEEZENET 1.1 (IANDOLA ET AL., 2016)	1.2	1	4.6	2.3	1.15	0.58
		10	46.0	23.0	11.5	5.8
		100	460	230	115	58
SHUFFLENET V2 (MA ET AL., 2018)	2.3	1	8.8	4.4	2.2	1.1
		10	88.0	44.0	22.0	11.0
		100	880	440	220	110
MOBILENETV3-SMALL (HOWARD ET AL., 2019)	2.5	1	9.5	4.8	2.4	1.2
		10	95.0	48.0	24.0	12.0
		100	950	480	240	120
MOBILENETV2 (SANDLER ET AL., 2018)	3.4	1	13.0	6.5	3.25	1.63
		10	130	65.0	32.5	16.3
		100	1300	650	325	163
MNASNET 1.0 (TAN ET AL., 2018)	3.9	1	14.9	7.45	3.73	1.86
		10	149	74.5	37.3	18.6
		100	1490	745	373	186
MOBILENETV1 (HOWARD ET AL., 2017)	4.2	1	16.0	8.0	4.0	2.0
		10	160	80.0	40.0	20.0
		100	1600	800	400	200
EFFNET-LITE0 (TAN & LE, 2019)	4.7	1	17.9	8.95	4.48	2.24
		10	179	89.5	44.8	22.4
		100	1790	895	448	224
GOOGLENET (SZEGEDY ET AL., 2015)	6.6	1	25.2	12.6	6.3	3.15
		10	252	126	63.0	31.5
		100	2520	1260	630	315
RESNET-18 (HE ET AL., 2016)	11.7	1	44.6	22.3	11.2	5.58
		10	446	223	112	55.8
		100	4460	2230	1115	558
RESNET-50 (HE ET AL., 2016)	25.6	1	97.7	48.9	24.4	12.2
		10	977	489	244	122
		100	9770	4890	2440	1220
CONVNEXT-TINY (LIU ET AL., 2022)	28.6	1	109	54.5	27.3	13.6
		10	1090	545	273	136
		100	10900	5450	2730	1360

Table 4. Communication efficiency analysis on the CIFAR-10 dataset. The table reports the total communication rounds required to reach specific accuracy thresholds. **Norm. Rounds** denotes the communication cost relative to FEDADAVR (e.g., a value of 2.0 means the method took twice as many rounds as FEDADAVR). 'x' indicates the target was not reached.

STRATEGY	CRITERIA	ACCURACY					
		20 %	25 %	30 %	35 %	40 %	45 %
FEDAVG	ROUNDS	335	488	619	823	1324	1396
	NORM. ROUNDS	3.3	2.3	2.1	2.0	2.0	1.5
FEDADAGRAD	ROUNDS	355	646	988	1368	x	x
	NORM. ROUNDS	3.5	3.1	3.3	3.2	x	x
FEDADAM	ROUNDS	x	x	x	x	x	x
	NORM. ROUNDS	x	x	x	x	x	x
FEDYOGI	ROUNDS	478	727	1066	1483	x	x
	NORM. ROUNDS	4.7	3.5	3.6	3.5	x	x
FEDPROX	ROUNDS	338	484	726	921	1193	x
	NORM. ROUNDS	3.3	2.3	2.5	2.2	1.8	x
SCAFFOLD	ROUNDS	x	x	x	x	x	x
	NORM. ROUNDS	x	x	x	x	x	x
FEDNOVA	ROUNDS	338	612	734	1082	1352	1491
	NORM. ROUNDS	3.3	2.9	2.5	2.6	2.0	1.6
MIFA	ROUNDS	444	596	1012	x	x	x
	NORM. ROUNDS	4.4	2.9	3.4	x	x	x
FEDVARP	ROUNDS	116	204	427	566	878	1385
	NORM. ROUNDS	1.1	1.0	1.4	1.3	1.3	1.5
FEDADAVR-QUANT	ROUNDS	189	284	343	554	803	1118
	NORM. ROUNDS	1.9	1.4	1.2	1.3	1.2	1.2
FEDADAVR	ROUNDS	101	209	296	421	661	918
	NORM. ROUNDS	1.0	1.0	1.0	1.0	1.0	1.0

Table 5. Computational latency analysis on the CIFAR-10 dataset (IID partition). We report the average wall-clock time (in seconds) required for a single communication round. For FEDADAVR, we detail the latency incurred when employing different server-side optimisers.

ALGORITHM	SERVER OPTIMISER	TIME (SECONDS)
FEDAVG	x	166.43
FEDADAM	x	168.32
FEDADAGRAD	x	167.89
FEDYOGI	x	168.54
FEDPROX	x	170.57
SCAFFOLD	x	184.89
FEDNOVA	x	168.65
MIFA	x	172.58
FEDVARP	x	175.27
FEDADAVR	ADAM	180.30
FEDADAVR	ADAGRAD	178.31
FEDADAVR	ADABELIEF	181.53
FEDADAVR	YOGI	180.41
FEDADAVR	LAMB	183.15

Table 6. Accuracy comparison of FedVARP, FEDADAVR and FEDADAVR-QUANT algorithms on the Shakespeare dataset (Server learning rate: η_s).

ALGORITHM	OPTIMISER	η_s				
		0.001	0.005	0.01	0.1	1.0
FEDVARP	X	X	X	43.038	49.434	50.288
FEDADAVR	ADABELIEF	45.271	49.453	49.514	X	X
	ADAM	35.733	48.541	49.343	X	X
	ADAGRAD	38.379	50.048	50.577	X	X
	YOGI	27.921	48.440	49.549	X	X
	LAMB	42.057	41.034	31.383	X	X
FEDADAVR-QUANT	ADABELIEF	45.295	49.273	49.441	X	X
	ADAM	28.589	48.604	49.468	X	X
	ADAGRAD	41.492	50.065	50.611	X	X
	YOGI	43.501	48.470	49.507	X	X
	LAMB	41.799	41.201	41.556	X	X

Table 7. Accuracy comparison of FedVARP, FEDADAVR and FEDADAVR-QUANT algorithms on the MNIST dataset (Server learning rate: η_s).

ALGORITHM	OPTIMISER	η_s	PARTITION					
			IID		NON-IID		DIRICHLET	
			LQ-1	LQ-2	LQ-3	LQ-4	LQ-5	LQ-6
FEDVARP		0.01	11.948	12.378	10.896	7.110	13.158	8.679
		0.1	33.715	10.095	11.200	18.558	11.386	19.194
		1.0	90.604	89.336	80.284	73.246	70.984	78.185
FEDADAVR	ADABELIEF	0.001	93.106	90.913	84.935	69.180	77.921	83.236
		0.005	96.535	96.271	90.653	80.156	90.300	92.319
		0.01	96.472	94.311	88.223	29.601	86.857	92.168
FEDADAVR	ADAM	0.001	89.946	88.965	79.936	59.161	74.584	82.445
		0.005	95.827	95.524	94.710	75.651	84.957	85.931
		0.01	97.053	95.763	94.093	50.326	78.899	94.384
FEDADAVR-QUANT	ADAGRAD	0.001	80.725	73.430	58.210	33.542	55.089	46.129
		0.005	91.595	90.680	89.272	53.171	78.550	84.840
		0.01	92.781	93.171	92.540	61.943	83.394	87.941
FEDADAVR-QUANT	LAMB	0.001	38.891	16.909	14.176	19.574	19.274	12.740
		0.005	77.128	65.159	62.869	57.072	50.162	64.278
		0.01	90.108	85.646	82.008	81.884	77.998	75.294
FEDADAVR-QUANT	YOGI	0.001	89.739	89.105	78.241	49.335	71.816	83.518
		0.005	95.368	95.470	92.924	82.808	88.219	92.986
		0.01	96.657	94.929	93.644	60.528	86.690	93.480
FEDADAVR-QUANT	ADABELIEF	0.001	93.656	91.219	85.578	70.892	67.061	84.328
		0.005	96.280	96.205	92.165	68.557	87.636	92.688
		0.01	96.651	95.655	93.691	52.374	90.604	92.991
FEDADAVR-QUANT	ADAM	0.001	89.497	88.650	80.970	71.772	68.054	82.382
		0.005	95.793	96.128	93.778	67.327	81.980	93.727
		0.01	96.906	95.740	85.748	23.238	89.085	94.135
FEDADAVR-QUANT	ADAGRAD	0.001	80.639	65.572	49.605	37.277	39.020	48.227
		0.005	91.780	91.749	83.913	52.490	75.974	86.978
		0.01	94.542	93.183	90.082	69.314	81.980	78.666
FEDADAVR-QUANT	LAMB	0.001	21.756	21.453	17.390	19.582	16.890	18.872
		0.005	78.681	72.762	65.166	49.364	58.694	54.940
		0.01	88.685	85.356	85.297	79.123	77.519	82.170
FEDADAVR-QUANT	YOGI	0.001	91.659	89.871	74.876	45.566	74.133	84.271
		0.005	96.286	95.496	91.644	73.522	83.347	91.729
		0.01	96.023	83.088	90.476	52.479	84.424	92.483

Table 8. Accuracy comparison of FedVARP, FEDADAVR and FEDADAVR-QUANT algorithms on the FMNIST dataset (Server learning rate: η_s).

ALGORITHM	OPTIMISER	η_s	PARTITION					
			IID	NON-IID	DIRICHLET	LQ-1	LQ-2	LQ-3
FEDVARP		0.01	10.009	10.376	10.003	14.467	30.655	16.861
		0.1	60.217	60.506	63.441	44.840	56.687	58.473
		1.0	79.861	77.533	77.159	59.830	66.604	72.406
FEDADAVR	ADABELIEF	0.001	77.206	75.723	75.479	60.533	70.333	71.190
		0.005	83.068	80.808	82.506	69.568	73.317	77.437
		0.01	84.083	84.061	83.201	71.971	74.126	77.967
FEDADAVR	ADAM	0.001	75.104	74.047	83.091	63.023	68.741	66.983
		0.005	82.967	81.798	79.051	70.451	71.880	77.600
		0.01	84.133	83.317	73.935	69.601	73.890	78.187
FEDADAVR-QUANT	ADAGRAD	0.001	61.777	55.181	51.176	32.834	48.904	56.658
		0.005	75.536	74.302	73.287	52.836	69.273	71.135
		0.01	80.631	77.400	77.081	66.620	72.212	73.210
FEDADAVR-QUANT	LAMB	0.001	29.955	18.785	20.715	25.693	10.834	31.067
		0.005	64.062	62.505	68.601	59.870	57.882	60.637
		0.01	74.485	74.902	76.427	66.529	70.554	74.941
FEDADAVR-QUANT	YOGI	0.001	73.734	72.907	73.575	58.439	69.226	71.972
		0.005	82.278	80.929	81.844	68.520	75.177	77.557
		0.01	84.313	83.488	82.667	70.351	75.262	78.969
FEDADAVR-QUANT	ADABELIEF	0.001	76.771	75.066	75.925	61.089	70.575	69.917
		0.005	84.312	80.538	82.487	64.235	71.664	78.029
		0.01	84.842	82.479	83.256	67.758	76.298	79.775
FEDADAVR-QUANT	ADAM	0.001	83.627	71.554	73.351	64.843	65.539	71.405
		0.005	83.627	80.229	81.663	66.374	72.876	77.430
		0.01	83.286	83.372	82.759	67.422	74.908	80.083
FEDADAVR-QUANT	ADAGRAD	0.001	58.684	57.487	48.563	30.279	33.819	46.890
		0.005	75.566	73.364	74.482	55.513	66.891	70.554
		0.01	80.323	78.173	77.643	64.225	71.448	75.407
FEDADAVR-QUANT	LAMB	0.001	33.004	18.693	22.779	27.412	15.892	24.672
		0.005	62.429	65.230	69.666	60.410	59.479	69.687
		0.01	74.996	72.674	76.825	66.031	70.278	73.933
FEDADAVR-QUANT	YOGI	0.001	73.886	73.904	72.354	61.025	69.328	71.145
		0.005	83.067	80.675	80.393	69.802	72.447	77.480
		0.01	84.505	82.265	83.013	67.610	72.140	78.209

Table 9. Accuracy comparison of FedVARP, FEDADAVR and FEDADAVR-QUANT algorithms on the CIFAR-10 dataset (Server learning rate: η_s).

ALGORITHM	OPTIMISER	η_s	PARTITION					
			IID		NON-IID		DIRICHLET	
			IQ-1	IQ-2	IQ-3	IQ-4	IQ-5	IQ-6
FEDVARP		0.01	33.264	32.313	27.678	36.275	42.852	51.393
		0.1	51.886	51.629	47.239	38.955	41.848	49.376
		1.0	68.991	65.367	60.645	31.437	40.883	52.860
FEDADAVR	ADABELIEF	0.001	70.079	70.286	64.964	39.170	54.028	63.485
		0.005	66.879	67.349	60.335	33.196	46.427	53.842
		0.01	61.706	55.696	58.381	30.451	43.733	54.039
FEDADAVR	ADAM	0.001	67.733	69.564	65.697	37.922	54.314	64.917
		0.005	70.847	65.622	61.038	32.048	49.253	56.156
		0.01	61.148	61.587	56.812	35.590	47.334	54.656
FEDADAVR-QUANT	ADAGRAD	0.001	59.793	58.641	54.630	42.789	50.628	55.925
		0.005	68.148	67.409	65.214	36.303	49.304	56.691
		0.01	54.224	60.239	57.613	35.699	44.933	53.007
FEDADAVR-QUANT	LAMB	0.001	54.684	58.506	55.179	46.708	51.095	55.157
		0.005	67.391	68.028	62.049	39.746	55.811	65.776
		0.01	71.228	68.186	67.800	32.201	53.038	62.611
FEDADAVR-QUANT	YOGI	0.001	70.111	68.121	64.132	37.197	59.574	66.144
		0.005	65.009	67.969	57.988	30.859	46.552	58.175
		0.01	72.031	59.232	67.178	43.264	56.090	65.202
FEDADAVR-QUANT	ADABELIEF	0.001	69.752	67.974	66.877	44.098	57.287	65.879
		0.005	63.308	64.362	59.331	34.306	45.823	55.755
		0.01	61.706	59.579	58.075	29.796	42.272	60.404
FEDADAVR-QUANT	ADAM	0.001	67.959	69.564	64.900	41.006	59.393	67.559
		0.005	64.207	65.291	60.126	35.561	50.557	65.648
		0.01	63.218	64.080	55.995	35.133	48.095	51.586
FEDADAVR-QUANT	ADAGRAD	0.001	59.416	59.310	55.321	45.397	50.277	55.364
		0.005	68.148	68.293	62.896	46.895	54.594	63.775
		0.01	55.541	61.392	59.302	44.533	48.300	56.199
FEDADAVR-QUANT	LAMB	0.001	54.947	57.840	54.903	46.784	53.491	58.537
		0.005	69.562	67.456	67.230	37.764	59.843	67.896
		0.01	73.364	69.175	68.555	34.379	57.870	63.666
FEDADAVR-QUANT	YOGI	0.001	70.322	67.564	65.747	42.870	58.615	65.741
		0.005	65.668	63.411	61.825	37.073	55.960	63.561
		0.01	59.972	63.330	67.230	46.784	58.634	64.014